AD-A110 036 LOCKHEED-GEORGIA CO MARIETTA F/G 20/4
NUMERICAL AIRCRAFT DESIGN USING 3-D TRANSONIC ANALYSIS WITH OPT--ETC(U)
AUG 81 P AIDALA F33615-78-C-3014
UNCLASSIFIED L681ER0107-VOL-2-PT-2 AFWAL-TR-81-3091-VOL-2-PT- NL

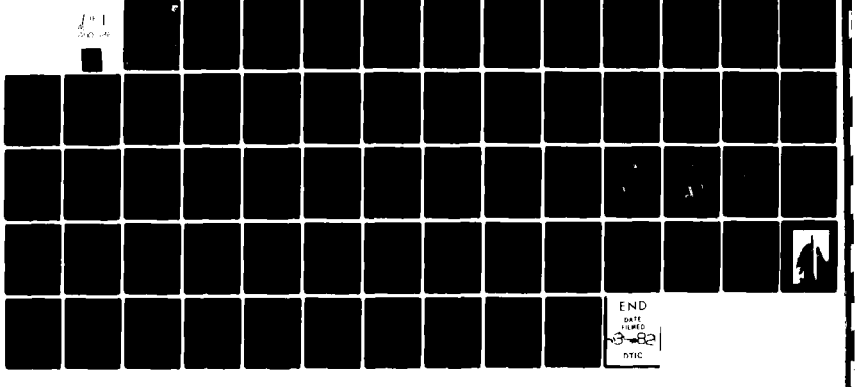

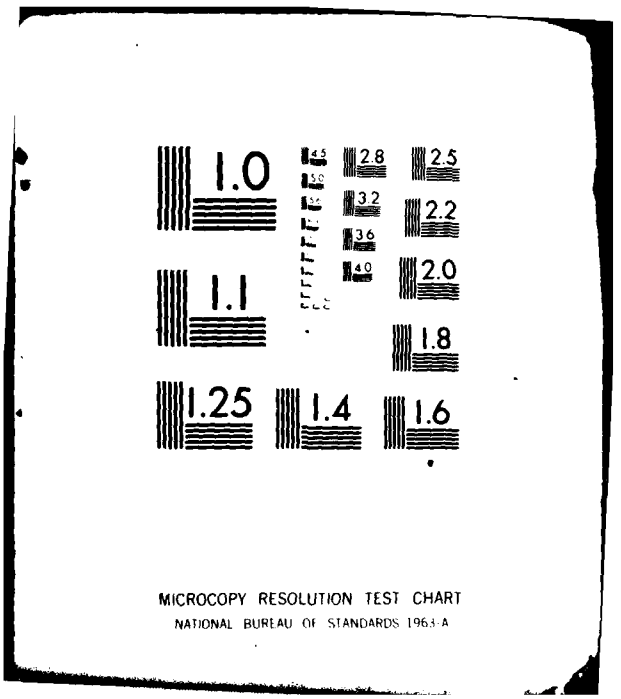
1.0
1.1
1.25
1.4
1.6
1.8
2.0
2.2
2.5
2.8
3.2
3.6
4.0
MICROCOPY RESOLUTION TEST CHART
NATIONAL BUREAU OF STANDARDS 1963-A

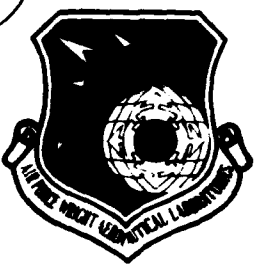

AFWAL-TR-81-3091
VOLUME II, PART 2

NUMERICAL AIRCRAFT DESIGN USING 3-D TRANSONIC ANALYSIS WITH OPTIMIZATION

VOLUME II
PART 2: FIGHTER DESIGN

Lockheed-Georgia Company
86 South Cobb Drive
Marietta, Georgia 30063

Grumman Aerospace Corporation
Bethpage, New York 11714

August 1981

Final Report May 1978 to September 1980

Flight Dynamics Laboratory
Air Force Wright Aeronautical Laboratories
Air Force Systems Command
Wright-Patterson Air Force Base, Ohio 45433

NOTICE

When Government drawings, specifications, or other data are used for any purpose other than in connection with a definitely related Government procurement operation, the United States Government thereby incurs no responsibility nor any obligation whatsoever; and the fact that the government may have formulated, furnished, or in any way supplied the said drawings, specifications, or other data, is not to be regarded by implication or otherwise as in any manner licensing the holder or any other person or corporation, or conveying any rights or permission to manufacture use, or sell any patented invention that may in any way be related thereto.

This report has been reviewed by the Office of Public Affairs (ASD/PA) and is releasable to the National Technical Information Service (NTIS). At NTIS, it will be available to the general public, including foreign nations.

This technical report has been reviewed and is approved for publication.

Robert A. Large

ROBERT A. LARGE, Capt, USAF
Project Engineer

Lowell C. Keel

LOWELL C. KEEL, Maj, USAF
Chief, Aerodynamics & Airframe Branch
Aeromechanics Division

FOR THE COMMANDER

J. R. Chevalier

JOHN R. CHEVALIER, Colonel, USAF
Chief, Aeromechanics Division

"If your address has changed, if you wish to be removed from our mailing list, or if the addressee is no longer employed by your organization please notify AFWAL/FIMM, *W-PAFB, OH 45433 to help us maintain a current mailing list".*

Copies of this report should not be returned unless return is required by security considerations, contractual obligations, or notice on a specific document.

AIR FORCE/56780/11 December 1981 — 180

SECURITY CLASSIFICATION OF THIS PAGE (When Data Entered)

REPORT DOCUMENTATION PAGE	READ INSTRUCTIONS BEFORE COMPLETING FORM
1. REPORT NUMBER: AFWAL-TR-81-3091 Volume II, Part 2	2. GOVT ACCESSION NO.: AD-A110 036
	3. RECIPIENT'S CATALOG NUMBER:
4. TITLE (and Subtitle): NUMERICAL AIRCRAFT DESIGN USING 3-D TRANSONIC ANALYSIS WITH OPTIMIZATION VOLUME II, PART 2: FIGHTER DESIGN	5. TYPE OF REPORT & PERIOD COVERED: Final Report May 1978 - September 1980
	6. PERFORMING ORG. REPORT NUMBER: LG81ER0107
7. AUTHOR(s): P. Aidala	8. CONTRACT OR GRANT NUMBER(s): F33615-78-C-3014
9. PERFORMING ORGANIZATION NAME AND ADDRESS: Grumman Aerospace Corporation Bethpage, New York 11714	10. PROGRAM ELEMENT, PROJECT, TASK AREA & WORK UNIT NUMBERS: 62201F 24041026
11. CONTROLLING OFFICE NAME AND ADDRESS: Flight Dynamics Laboratory (AFWAL/FIMM) Air Force Wright Aeronautical Laboratories Wright-Patterson Air Force Base, Ohio 45433	12. REPORT DATE: August 1981
	13. NUMBER OF PAGES: 56
14. MONITORING AGENCY NAME & ADDRESS(if different from Controlling Office)	15. SECURITY CLASS. (of this report): Unclassified
	15a. DECLASSIFICATION/DOWNGRADING SCHEDULE

16. DISTRIBUTION STATEMENT (of this Report)

Approved for public release; distribution unlimited

17. DISTRIBUTION STATEMENT (of the abstract entered in Block 20, if different from Report)

18. SUPPLEMENTARY NOTES

Prepared in cooperation with Lockheed-Georgia Company

19. KEY WORDS (Continue on reverse side if necessary and identify by block number)

Aircraft	Optimization	Transonic Flow Analysis
Aerodynamics	Wing Design	Numerical Optimization
Canard Configuration	Computational Aerodynamics	
Transonic Flow	Transonic Aircraft Design	

20. ABSTRACT (Continue on reverse side if necessary and identify by block number)

The results of a fighter design case study performed to evaluate the transonic aircraft design procedure developed as part of the Advanced Transonic Technology (ATT) program are presented. The fighter design is based on the Configuration Design of Advanced Fighters program dual role configuration. Extensive wind tunnel testing of the design configuration was performed to validate the design procedure. The results of the wind tunnel tests are correlated with computational results generated in the design process.

DD FORM 1 JAN 73 1473 EDITION OF 1 NOV 65 IS OBSOLETE S/N 0102-014-6601 |

Unclassified

SECURITY CLASSIFICATION OF THIS PAGE (When Data Entered)

20. ABSTRACT (continued)

The purpose of the ATT program was to develop and validate a new transonic wing design procedure using numerical optimization. The new procedure was used to design both a transport and a fighter configuration. Because the missions and design requirements of a fighter and transport are so different, the design procedure was developed along parallel lines.

This is Part 2 of a two-part volume: Part 1 details the transport development, and Part 2 describes the fighter development. There are two other volumes which make up the final report. Volume 1 is an executive summary. It highlights the information that has been presented in detail here. Volume 1 is also divided into two parts with Part 1 dealing with transport design and Part 2 concerned with the fighter design. Volume 3 is a detailed user's guide to the computer programs produced under this contract. Volume 3 is similarly divided into two parts.

PREFACE

This document reports results obtained by the Lockheed-Georgia Co. and Grumman Aerospace Corp. under AFFDL Contract # F33615-78-C-3014. The purpose of the contract was to deveop and validate a new transonic wing design procedure using the numerical optimization technique. The new procedure was used to design both a transport and a fighter configuration.

Because the missions and design requirements of a fighter and transport are so different, the design procedure was developed along parallel lines. Lockheed-Georgia Co. developed the transport design procedure, and Grumman Aerospace Corp. did the fighter design.

This is Part 2 of a two-part volume: Part 1 details the transport development, and Part 2 describes the fighter development. There are two other volumes which make up the final report. Volume 1 is an executive summary. It highlights the information that has been presented in detal here. Volume 1 is also divided into two parts with Part 1 dealing with transport design and Part 2 concerned with the fighter design. Volume 3 is a detailed user's guide to the computer programs produced under this contract. Volume 3 is similarly divided into two parts.

Personnel who contributed to this contract effort are: Lockheed-Georgia Company, A. J. Srokowski, M. E. Lores, R. A. Weed and P. R. Smith; Grumman Aerospace Corp., P. Aidala. The authors also wish to acknowledge the assistance given by Capt. R. A. Large who was the AFWAL contract monitor.

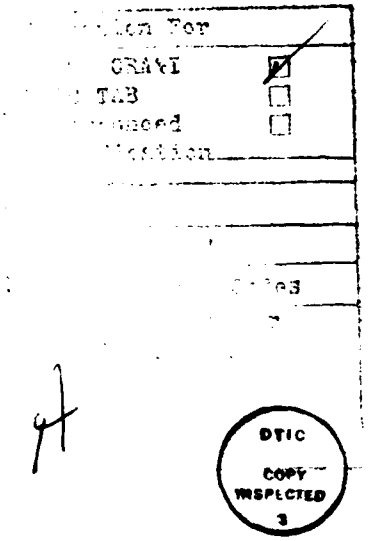

TABLE OF CONTENTS

LIST OF ILLUSTRATIONS

LIST OF ILLUSTRATIONS (Cont'd.)

2

SECTION I

INTRODUCTION

Computational aerodynamic methods for the design of future configurations are becoming more important. New technology concepts and new configurational concepts are being developed to improve transonic performance. Accurate performance predictions are needed to confidently evaluate the benefits of new concepts. In addition, the pursuit of increased performance and reduced development time and costs intensify the use of three-dimensional computational analysis.

Significant strides have been made in the development of 3-D transonic aerodynamic design and analysis codes over the past five years. Although many of the methods are still in the evolutionary status, some have matured to the point that they can be applied to the solution of practical aircraft problems. However, application of these methods to real aircraft design problems has occurred only to a limited degree. The primary objective of the study reported here is to demonstrate that performance improvements and/or reduced development time and costs can be achieved by incorporating 3-D transonic methods into fighter aircraft design procedures. The basic approach used is to couple a 3-D transonic analysis code with numerical optimization. Numerical optimization was chosen because it provides the greatest flexibility of design problem definition and analysis code selection. A goal of this study is to develop a user-oriented, reliable, accurate design methodology of general applicability.

The report is structured in a chronological manner, with each section corresponding to a technical task. Six technical tasks were performed in three time phases. During Phase I, an advanced fighter configuration was selected (Task 1). Also, the available 3-D transonic codes were evaluated, and modified for the configuration analysis and design procedure use (Task 2). Phase II consisted of the detailed aerodynamic design and wind tunnel test of the selected configuration (Task 3). Three technical tasks occurred in Phase III: computational and experimental results were evaluated (Task 4); the design methodology benefits were evaluated (Task 5) and a final design procedure was developed (Task 6).

Computer time for the results shown here was provided by NASA Ames Research Center on a CDC 7600. In addition, parts of the work were performed at NASA Ames through the Grumman-Ames Research Program Associate Program.

SECTION II

FIGHTER CONFIGURATION SELECTION

The Configuration Development of Advanced Fighters (CDAF) dual-role concept [1] was selected for the fighter design methodology development. The criteria for its selection were: the ability to perform existing and future Air Force missions with significant performance improvements over existing aircraft, the incorpration of advanced technology and the potential to benefit from a new 3-D transonic design methodology. The CDAF configuration satisfies all these criteria.

1. MISSION PERFORMANCE

Several studies of the interaction of mission requirements, technology advancements and weapon system configurations have shown the need for supersonic dash rather than today's transonic cruise, through enemy airspace [2]. An objective of the Configuration Development of Advanced Fighters study was to derive, evaluate, analyze and test an advanced supersonic cruise fighter.

The Configuration Development of Advanced Fighters preferred concept embraces efficient supersonic capability, high levels of maneuverability, basing versatility, weapon carriage flexibility, and observables management - five key ingredients required for the success of a "next-generation" tactical fighter. The concept is responsive to future Air Force weapon system design issues, has excellent mission performance characteristics and has been extensively documented in wind tunnel and radar cross section tests.

The preferred concept developed in the CDAF study is shown in Figure 1. The CDAF preferred concept is a dual-role vehicle developed for the fighter maneuvering role, emphasizing air-to-air capability (Fighter) with designed-in flexibility for adequate air-to-ground performance (Penetrator). The key performance characteristics are presented in Table 1.

TABLE 1. CDAF DUAL-ROLE CONCEPT PERFORMANCE SUMMARY

	FIGHTER	PENETRATOR	
TAKEOFF GROSS WEIGHT, LB	26,690	32,107	34,207
W/S AT TOGW, PSF	59	71	76
T/W AT TOGW	1.09	0.91	0.85
WEAPON PAYLOAD, LB	4 X 250	4 X 500	2 X 2000
FUEL, LB	7,382	11,372	11,372
FUEL FRACTION	0.28	0.35	0.33
CRUISE MACH*	0.9/1.6	0.9/2.0	0.9/2.0
CRUISE RADIUS*, N MI	100/250	474/200	365/200
CRUISE ALTITUDE*, K FT	50.0/65.6	50.0/66.5	50.0/66.8
CRUISE L/D*	12.6/7.2	12.6/6.3	12.6/6.3
CRUISE SFC*, LB/HR/LB	1.18/1.41	1.17/1.53	1.17/1.53
CRUISE RANGE FACTOR*, $\frac{M\ (L/D)}{SFC}$	9.6/8.2	9.7/8.2	9.7/8.2
SUST G, M .9/30K FT**	5.0	3.8	3.5
SUST G, M 1.6/50K FT	3.2	3.1	2.7
ACCEL. M .9 TO M 1.6, 30K FT, SEC	44	54	62
TAKEOFF GROUND ROLL, FT	475	760	875
LANDING GROUND ROLL, FT	850	975	996

* SUBSONIC/SUPERSONIC CRUISE (PERFORMANCE ON RETURN LEG)
** 50% FUEL IN FIGHTER ROLE, 80% FUEL IN PENETRATOR ROLE

The dual-role CDAF concept is a single-place, flat-bottom, twin-engine, canard-wing aircraft configured for relaxed static stability. The engines are podded separately beneath the low wing with two-dimensional nozzles located at the wing trailing edge. Other factors central to the design philosophy are weapon carriage flexibility, low observables, high-alpha control and safe engine operation, and 360-degree ECM coverage.

The aircraft was balanced 15% unstable at transonic speeds to minimize trim drag at transonic maneuver, resulting in neutrally stable supersonic flight. A small fixed glove extends from the wing to the canard pivot, merging with the local fuselage lines at the pivot station. The resultant fuselage cheek and glove enhances the cross-sectional area progression between the canard and the wing. This cheek-glove provides volume for the forward and side aspect electronic counter measure installation, gun breech and ammunition feed mechanism, forward fuel and the main landing gear wheels.

Smooth-skin, variable-camber leading and trailing flaps are incorporated on the wing. The chord ratio of the leading edge device increases toward the tip, while that of the trailing edge flap increases toward the root. This system enables simultaneous variations of wing camber and twist to produce efficient countours throughout the flight envelope. Two virtual hinges are used to produce the appropriate deflections in the inboard trailing edge and outboard leading edge flap regions. A low-set, all-flying canard is located slightly above the wing chord plane. The canard is attached to, and pivots about, the nose landing gear bulkhead.

A single vertical tail is mounted on the aft-fuselage section. High-aspect ratio was utilized, not only for the direct aspect ratio benefits, but also to locate some tail area in the favorable sidewash field above the canard and wing wakes at high angles-of-attack. A long dorsal is introduced to improve vertical tail effectiveness at high yaw angles. The dorsal strake also complements the cross-sectional area progression throughout this region.

Wind tunnel data verify that the CDAF preferred concept represents a significant advancement in combining supersonic cruise and transonic maneuver capability. Figure 2 shows that transonic maneuver acceleration and supersonic cruise lift-to-drag ratio are both increased by 60% relative to current aircraft capability.

2. ADVANCED TECHNOLOGY DEPENDENCE

The implementation of advanced technology in the CDAF concept is shown in Figure 3. The benefits of this technology are illustrated in Figure 4. The figure shows the resulting takeoff gross weight (TOGW) increase when a technology component is "removed" from the configuration. A "conventional concept" cannot perform the CDAF design mission. When all of the advanced technologies are removed, the aircraft weight estimates show the fuel needed exceeds the fuel available and the TOGW calculation diverges. The incorporation of advanced technology in the CDAF preferred concept is crucial to obtaining adequate performance for a supersonic cruise air combat mission representative of future tactical aircraft requirements.

3. DESIGN METHODOLOGY BENEFIT

The maximum benefits of a transonic design methodology result when the most challenging performance goals are pursued. Maximum transonic maneuver performance for a supersonic aircraft represents the challenge. This cannot be considered simply as enhancement of a contemporary air combat fighter. Transonic maneuver requirements call for a relatively low wing loading and a moderately swept, high aspect ratio wing while supersonic cruise efficiency demands relatively high wing loading and a thin, highly swept, low aspect ratio wing. These requirements dictate the most advanced transonic variable camber wing/airfoil technology available to resolve this "conflict". Maneuver wing design technology is the major design driver to minimize the cruise/maneuver wing sizing mismatch. This class of wing must embody spanwise varying airfoils and unique variable camber requirements if it is to meld good supersonic cruise performance with outstanding maneuvering capability. The primary aerodynamic need is to develop 3-D transonic design procedures to handle this nonuniform geometry.

SECTION III

SELECTION AND DEVELOPMENT OF METHODS

The key element of the design methodology is a 3-D transonic analysis code combined with numerical optimization. A new wing-body-canard transonic analysis capability was developed. Numerical optimization was chosen as part of the design methodology because it provides the greatest flexibility of design problem definition and analysis code selection. Numerous 2-D and 3-D applications have demonstrated the advantages of this approach.

1. ANALYSIS CODE DEVELOPMENT

The basic computational method employed in the transonic code analysis is that of Boppe [3]. An earlier version (1978) of the wing-body analysis code was used as the base on which to develop the wing-body-canard analysis capability. The key attraction of the Boppe code is its "nested mesh" technique. The flexibility of the nested mesh technique for configuration analysis hs been demonstrated in References [3] through [7]. In particular, a pilot wing-canard capability was demonstrated in Reference [4]. Figure 4 illustrates the nested mesh technique for a wing-body-canard configuration.

The flow equation used in the analysis is an "extended" small disturbance equation:

$$(1-M_\infty^2 - (\gamma+1)M_\infty^2\phi_x - \frac{\gamma+1}{2} M_\infty^2\phi_x^2)\phi_{xx} - 2M_\infty^2\phi_y\phi_{xy} + (1-(\gamma-1)M_\infty^2\phi_x)\phi_{yy} + \phi_{zz} = 0 \qquad (1)$$

Additional terms have been added to the classical small-disturbance equation to better capture swept shock waves and more accurately determine the critical velocity. Empirical modifications and similarity variables are not employed.

The original Boppe code employed a simple tangent function for the wing-body streamwise grid transformation. This transformation results in a sparse grid point distribution where a canard may be located. Simple perturbations of the tangent function would not accommodate arbitrary canard size and placement. Thus, a completely new streamwise grid transformation was developed.

The streamwise grid transformation used for wing-canard planforms is:

$$X = a_0 + a_1\xi + a_2\xi^2 + a_3\xi^3 + a_4\xi^4 + a_5\xi^5 + a_s\xi/(1-\xi^2) \qquad (2a)$$

$$\xi = \xi/\xi_\infty \qquad (2b)$$

This transforms the finite domain $-1 \leq \xi \leq 1$ to the infinite region $-\infty \leq X \leq \infty$. The constant a_s is empirical, controlling the rate of stretching near infinity. The points at $\xi = \pm 1$ are made the points of maximum density of mesh planes by specifying the second derivative of X to be zero. The value of X and the first derivative of X at $\xi = \pm 1$ are also specified to determine the coefficients a_0 to a_5. The value of ξ_∞ is adjusted iteratively to place approximately fifty percent of the total mesh planes between the most forward and the most aft points on the wing-canard combination.

For an aft swept wing-canard combination, the wing tip and canard tip determine the transformation coefficients. An example of the resulting wing-canard grid transformation and the corresponding physical mesh plane distribution is shown in Figure 6. The mesh transformation has been applied to several aft-swept configurations, several forward-swept configurations and to several arbitrary wing-canard parametric variations. Good results were observed in all cases. For forward swept wings, the canard tip and wing tip may be near the same streamwise location. In this case, wing/canard tip locations and the trailing edge of the centerline of the wing are used to determine the transformation coefficients.

The grid transformations for the spanwise and vertical meshes were simple perturbations of the original wing-body transformations. The perturbations adjust the spanwise grid so as to place both the wing and canard tip midway between mesh planes. The vertical grid is adjusted so that the canard and wing are each coincident with a mesh plane.

Individual embedded fine grid arrays are constructed for the wing and canard at each position where a crude spanwise mesh plane intercepts the wing and canard surfaces. These secondary mesh systems serve two purposes. First, detailed computations are performed only in a region very close to the surface where gradients are large and details are important. The resulting numerical efficienty permits a very dense computational mesh, a benefit in both the resolution of shock waves and the calculation of configuration forces and moments. Second, the embedded mesh systems are independent and sized for a particular geometric component. The system is not constrained by a single geometry-fitting

transformation. Thus, the sweep and taper of the wing does not effect the canard fine grid system and the canard sweep and taper does not effect the wing fine grid systems (see Figure 5). The fine grid arrays are evenly spaced in the vertical and streamwise directions.

The numerical solution of the flow equation uses successive line over-relaxation (SLOR). With two lifting surfaces and their attendant wakes, the basic algorithm for the SLOR solution was modified. The current capability of the code is an above wing, non-overlapping canard. As sketched in Figure 7, nine distinct flow-field regions for vertical line relaxation occur in the global crude grid:

Region 1 - Bounded by top and bottom infinity
Region 2 - Bounded by the canard and top infinity
Region 3 - Bounded by bottom infinity and the canard
Region 4 - Bounded by the canard wake and top infinity
Region 5 - Bounded by bottom infinity and the canard wake
Region 6 - Bounded by the wing and canard wake
Region 7 - Bounded by bottom infinity and the wing
Region 8 - Bounded by the wing wake and the canard wake
Region 9 - Bounded by bottom infinity and the wing wake

Similar SLOR regions are set up in the embedded fine grids. As indicated in Figure 7, the wakes are constraied to remain in the plane of the corresponding lifting surface. This is considered to be consistent with the other small disturbance approximations in the solution, but actually is also done in full potential codes. The error in this modeling is apparently negligible for a single lifting surface. However, when the wake of an upstream lifting surface comes arbitrarily close to a second surface, the influence of a wake model approximation may be significant. Unfortunately, detailed pressure data for simple wing-canard geometries does not exist to isolate this effect and evaluate the numerical model. Good predictions were obtained for the limited analyses done in this study.

The global crude grid has 51 streamwise, 26 spanwise and 31 vertical mesh planes (41,106 points). Eighteen spanwise planes fall between the symmetry plane and the wing tip. The number of spanwise planes intercepting the canard is proportional to the canard semispan. Each fine grid array can have up to 135 streamwise points and 25 vertical points, with 100 points on the airfoil chord. The code dimensions will allow up to 32 wing-canard fine grid arrays (108,000 points).

Viscous effects are computed in the analysis code by coupling a modified Bradshaw boundary layer computation with the inviscid potential flow solution. The boundary layer calculation is virtually identical to the method developed by Mason [8]. The method employs the modified chord technique of Nash [9] which represents an infinite sheared wing boundary layer calculation. The wing sweep angle is that of the local mid-chord span line, such that it may vary across the span. The 2-D Bradshaw turbulent boundary layer analysis [10] provides the

foundation for the method. The use of a modified 2-D boundary layer analysis greatly reduces the necessary computer time and has demonstrated good results for several different codes [3,8,11].

The boundary layer calculation provides a displacement thickness and skin friction calculation at each analysis station of the wing and canard. The slope of the displacement thickness is used to modify the surface boundary conditions in the inviscid solution. The local skin friction calculation is used to provide a viscous drag estimate for the configuration at the end of the analysis run.

The code analysis capability was evaluated with wind tunnel data for the CDAF configuration. Figure 8 shows results for three camber shapes. The amount of variable camber increase from the supersonic cruise (least camber) through transonic cruise to transonic maneuver (most camber). The code does not model the nacelles or vertical tail which are present in the data. Thirty counts of drag have been added to the analysis results. The computational mesh places fifteen analysis stations on the wing and eight analysis stations on the canard with eighty streamwise points on each airfoil section. Viscous effects are included with the boundary layer calculation described above. A typical computation requires approximately eleven minutes CPU time on a CDC 7600. A representative comparison of predicted and measured wing pressures is shown in Figure 9.

Comparisons of predicted wing pressure changes due to the canard on the CDAF supersonic cruise wing at Mach 0.9 are shown in Figure 10. Agreement between the predictions and data is good. Note that the change in pressures is significant only near the leading edge. This cannot be properly simulated with a simple local incidence change as is sometimes done with a wing-body analysis code to approximate the canard effect on the wing.

The wing-body-canard analysis code was coupled with the COPES and CONMIN routines of Vanderplaats [12,13]. The COPES code is a control program that connects the numerical optimization code CONMIN with the aerodynamic analysis code. The resulting computer code was named PANDORA-- Preliminary Automated Numerical Design Of Realistic Aircraft. The structure of the PANDORA code allows the numerical optimization to be coupled to any analysis code. Several "analysis" codes could be used together to provide information for the optimization. This information might be supersonic performance, TOGW changes or mechanical system sizing estimates. The available computer resources represent the only limit of complexity.

The computer code is written in FORTRAN, employing the CDC overlay structure. Storage requirements on a CDC 7600 are 151000_8 small core memory and 770000_8 large core memory. Typical CPU times on the 7600 for a wing-body-canard analysis with viscous effects is eleven minutes. The CPU time for an optimization run will vary according to the complexity of the optimization problem as discussed below.

The optimization algorithm within CONMIN is a modified Method of Feasible Directions [13]. The gradient information for the algorithm is calculated by sequentially perturbing each design variable. Each design variable perturbation requires analysis by the flow solution routines. Thus, the computer time is proportional to the number of design variables. The gradient information establishes a search direction that should improve the design (decrease the objective function) while satisfying any constraints. The search direction is "explored" until a relative optimum is found or any constraints become violated. If the starting conditions violated any constraints, the search direction will be that which satisfies the constraints with the least objective function increase. One to four flow solutions are required during the search. Completion of the search constitutes one optimization iteration.

2. DESIGN PROCEDURE DEVELOPMENT

Figure 11 illustrates the design procedure. The procedure defines a general systematic approach for any design problem that incorporates a transonic performance requirement. If the labels "transonic performance" and "non-transonic" were replaced with "design point" and "off-design", respectively, then the design procedure of Figure 11 can be applied to any aircraft mission performance design problem.

The design begins with a "conventional" wing design tailored to the particular requirements and philosophies of the specific configuration. Typically this is done using 2-D transonic and 3-D linear (subsonic and supersonic) computer codes. Then numerical optimization with a 3-D transonic code is used to refine the baseline wing geometry.

The numerical optimization requires the choice of design variables and optimization criteria. The key design variables control functions that modify the wing geometry. The optimization criteria consist of an objective function and constraints. The numerical optimization seeks to reduce the objective function (such as structural weight or aircraft drag). The constraints are conditions on the design (possibly none) that must be satisfied. Examples would be minimum fuel volume, maximum landing speed or minimum aircraft lift. The analysis code(s) evaluate the objective function and constraints for each design variable modification made by the optimization algorithm.

Two classes of geometry design functions are typical: piecewise wing section ordinate functions and complete wing section shape functions. Examples from 2-D applications can be found in References [14] and [15]. The piecewise ordinate functions are usually "bumps" and "wiggles" defined with polynomial, exponential or trigonometric functions. Each function modifies only a small area of the wing geometry at a single span station. With one design variable for each ordinate function, ths approach uses many design variables (20 to 60) for a complete wing design. The wing section shape functions modify all of the airfoil geometry at a single span station simultaneously. The different wing section shape functions may each be separate airfoils that the optimization "combines" to alter the wing geometry. Compared to the piecewise ordinate functions, the shape functions require a small number of design variables (10 to 20) for a wing

design. The fewer number of design variables not only reduces the necessary computer time but also makes it easier for the user to interpret the design variable changes made by the optimization.

Although the aerodynamic designer looks at aircraft performance to evaluate different aircraft, wing design optimization has often used a target pressure distribution as the optimization criteria. This avoids the uncertainties of calculated force and moments, but introduces the uncertainty of what is the optimum pressure distribution. This uncertainty is only amplified when off-design performance need be considered. Use of the calculated force and moments provides the aerodynamic designer with the easiest implementation and interpretation of the design optimization.

Transonic performance requirements are typically specified for cruise and maneuver conditions. The optimization criteria for transonic cruise would be minimum trimmed drag at the cruise lift coefficient. A pitching moment constraint could be used in place of explicitly calculating trimmed conditions. For transonic maneuver, the most appropriate optimization criteria would be maximum trimmed lift with a drag constraint (i.e., not more than the available thrust). Again, a pitching moment constraint can be used in place of calculating trimmed contitions. Transonic maneuver could use the same criteria as for cruise: minimum drag with lift and pitching moment constraints. As an objective function minimized by the optimization, the drag could be replaced by the square root of the drag or the negative of the lift to drag ratio. Insofar as these different drag formulas change the behavior of the objective function, different optimization results may occur.

If the criteria that determine the "best" configuration can all be evaluated with the 3-D transonic analysis, PANDORA can provide a self-sufficient design optimization. The particular constraints for a design optimization need be determined for the specific configuration (with its mission) that is being designed. Some constraints can be very simple, such as "mechanical" limits on the device deflections. These can be easily incorporated into the design variables and optimization function.

The design of realistic aircraft always involves a mission that includes non-transonic performance. Examples of non-transonic performance requirements are maximum lowspeed lift, supersonic cruise and supersonic maneuver. The transonic performance improvement may penalize the non-transonic performance. If so, the optimization function need be modified to include a "penalty factor" for the non-transonic performance penalty. Alternatively, the design variables may be modified to avoid or reduce the non-transonic performance penalty.

These modifications are determined external to the transonic analysis and optimization routines. The implementation of these modifications requires quantified numerical formulas. Typically the change in estimated takeoff gross weight (TOGW) is used to evaluate the trade between transonic and non-transonic performance. Then the "optimized" transonic performance with "satisfactory" non-transonic performance will be that which minimizes the aircraft TOGW while satisfying all the mission performance requirements.

An example of a supersonic cruise performance penalty for a transonic maneuver performance improvement is shown in Figure 12. In this example, only one design variable impacts the supersonic cruise (e.g., wing thickness, wing box twist) while the other design variables do not impact supersonic cruise (e.g., device deflections, angle of attack). The unconstrained transonic optimization produces a thirty count decrease in maneuver drag ($\Delta C_{D_{TM}}$) but results in a forty count increase in supersonic cruise drag ($\Delta C_{D_{SC}}$). This geometry produces a takeoff gross weight (TOGW) increase of two percent while the minimum TOGW would be a decrease of two percent. Two approaches can be used to direct the optimization to this result as shown in Figures 12a and 12b.

In Figure 12a the supersonic drag increase is evaluated for the geometry of the $\Delta C_{D_{TM}}$ minimum. The supersonic drag increase is approximated as a function of the design variable V. This is then used as a penalty formula that is added to the calculated transonic drag. The optimization becomes an approximation to the takeoff gross weight change (ΔTOGW). As an approximation, the optimized TOGW may not be the actual minimum TOGW. If so, more accurate approximations can be developed as more points are evaluated.

In Figure 12b, an approximate TOGW formula is used to estimate the optimum value of the design variable. After the initial transonic drag optimization, the design variable is constrained to an arbitrary value less than the original optimum. Then, with two results for the TOGW, a curve fit is used to estimate the value of the design variable for the TOGW minimum. The design variable is constrained to the estimated value and the cycle is repeated. As more points are evaluated, the approximated TOGW becomes more accurate.

SECTION IV

CONFIGURATION DESIGN AND WIND TUNNEL TEST

The configuration design provides a detailed demonstration and evaluation of the transonic design methodology. As applied to the CDAF configuration, the design goal was to reduce the takeoff gross weight by minimizing transonic maneuver drag while maintaining adequate supersonic performance. The wing tunnel test of the resulting geometries provides the data necessary to verify the analysis/optimization capability of the PANDORA code.

The force and moment results discussed in this section were those of the analysis code at the time of application. Several coding errors have been corrected since that time, which would change the calculated results. All analysis results discussed in other sections are from the most recent version of the code. The wing geometries from the numerical optimization discussed in this section might be different if rerun with the current analysis code.

1. BASELINE GEOMETRY ANALYSIS

The design of the baseline geometry (i.e., before any numerical optimization) began with linear supersonic and subsonic 3-D codes. The supersonic codes [16,17] were used to design the wing/canard camber, twist and thickness for minimum drag at supersonic cruise. The wing box geometry is then held fixed. (The canard geometry is held fixed, but with variable incidence available for trim.) The wing geometries for transonic cruise and maneuver were design by using subsonic codes [18,19] and wind tunnel data of a similar variable camber configuration [20,21]. No aeroelastic changes to wing box twist were assumed because the wing stiffness produces very small changes to wing box twist under load.

The starting geometry for the numerical optimization was the baseline transonic maneuver device deflections. At transonic maneuver conditions (Mach 0.9, C_L 0.7), wind tunnel data showed flow separation on the wing and canard that was well beyond the modeling capability of the code analysis. In order to reduce the extent of flow separation, the optimization was started at an angle of attack below that for the actual maneuver point. The flow solution at six degrees angle of attack (C_L 0.5) was chosen for the starting conditions.

A well-known drawback of numerical optimization in aerodynamic design is the computer time for the many aerodynamic analyses. The most accurate aerodynamic analysis would be a "converged" wing-body-canard solution, including viscous effects, for each geometry perturbation in the optimization search. The limits of computer resources for this study did not allow this. In order to reduce the computer time usage, the need for including the viscous effects and the canard influence during the wing design optimization were evaluated.

Analysis of the baseline configuration show little benefit of including a boundary layer model in the design process. The boundary layer would alter the magnitude of forces and moments, but it would not significantly change the relative influence of geometry perturbations. The numerical optimization uses the relative effects of geometry perturbations to choose the "best" design. The most significant effect of the boundary layer during the design would be flow separation. A fixed boundary layer shape (i.e., equivalent inviscid starting geometry) would not show any separation changes. If the flow separation were significant, then the boundary layer model is inadequate. If necessary, the boundary layer calculations could be included in the transonic analysis during optimization.

Evaluation of the canard influence (with both data and analysis) showed the only region of significant influence to be the forward part of the inboard wing sections. This region does not have any leading edge devices. Thus, the canard influence there could be considered as "interference pressures." Trim drag considerations could be included in the wing design by constraints or pitching moment penalty formulas. In general, the canard can be included in the transonic analysis for the optimization.

An additional change from the usual analysis in PANDORA was the use of a thinned mesh to further reduce computing times. The grid used placed twelve analysis stations on the exposed wing and fifty streamwise points on each wing section. Although the force and moment calculations are sensitive to grid changes, it was felt that the relative effect of the geometry perturbations would be adequately predicted. Thirty five flow solution iterations were used for the analysis of each geometry perturbation. The starting flow solution was the thinned-mesh, inviscid wing-body analysis results for the baseline geometry at six degrees angle of attack and 0.9 Mach number.

2. OPTIMIZATION FUNCTION DEFINITION

For aircraft design, the optimization function is that result of the aerodynamic analysis used to determine a "better" configuration. As applied to the CDAF configuration, the wing box geometry was not changed by the optimization procedure. With the wing box geometry held fixed, the technique of "optimizing" for a target pressure distribution does not provide a general method to determine the best transonic performance. The transonic performance itself need be the criteria for determining the optimum design. The capability to accurately and efficiently predict the transonic performance becomes crucial to the success of the numerical optimization. In general, the optimization problem for the "best" supersonic cruise fighter need consider the trade between more efficient transonic performance and more efficient supersonic cruise. This trade is evaluated through a take-off gross weight (TOGW) sensitivity for changes in transonic and supersonic performance of the particular configuration with its mission requirements. Consequently, it would be necessary to have accurate and efficient predictions of both transonic and supersonic performance for a successful design optimization.

It was the original intent of this study to investigate the trade between supersonic cruise and transonic maneuver performance. Initial application of two supersonic codes [16,22] did not reliably predict test data for the baseline configuration. In addition, the TOGW increase for a supersonic cruise drag increase was more than five times the TOGW decrease for a transonic maneuver drag decrease. (A wing geometry change that results in a five count supersonic drag increase would need to produce more than a twenty-five count transonic maneuver drag decrease for no change in TOGW).

The supersonic performance prediction uncertainty together with the TOGW sensitivity made a supersonic/transonic performance trade optimization impractical. The resulting design problem for numerical optimization was to determine the "best" variable camber shape for transonic maneuver. The usual numerical optimization problem was to reduce the drag, subject to the constraints of not decreasing the lift or pitching moment. Alternative optimization problems used were to minimize the square root of the drag, with lift and pitching moment constraints, and to maximize the lift, with moment and drag constraints.

3. DESIGN VARIABLE DEFINITON

Examples from earlier airfoil aerodynamic optimizations [14,15] used two types of design functions: piecewise polynomial shape functions and complete wing section shape functions. Two design approaches, corresponding to these two types of design functions were used.

Initially, a "camber" approach was used--the design variables were a mathematical representation of the variable camber device geometry. The variable camber segmentation is shown in Figure 13. Figure 14 illustrates the equation relating a design variable V(N) to a "device deflection" Z(N). The equations used represent the classical solution of a deflected, cantilevered beam. Small deflections are assumed, so that changes in the device arc length are ignored. This choice of design variables does not penalize the supersonic performance since the wing geometry can return to the supersonic cruise shape. (There were no mechanical limits imposed on the deflections.) Additional design variables could be incorporated by subdividing the variable camber segments.

Originally, eleven design variables were used to "deflect" the wing devices as sketched in Figure 15. A twelfth design variable was used to change the angle of attack. Later, sixteen design variables were used by subdividing four of the original camber segments. The four most outboard segments were subdivided first (segments 8-11 in Figure 15) and then, separately, the four most inboard segments were subdivided (segments 1-4 in Figure 15). The starting wing geometry was the transonic maneuver shape of the baseline configuration.

The second approach was a wing section "shape" approach. At each of the five defining span stations in Figure 15, two complete wing section shapes were specified and the optimization determined the best linear combination of the two shapes. The design variable at each span station represents the weighting factor for combining the two shapes, as shown in Figure 16. One of the sets of shapes used was the baseline transonic cruise wing sections. The other set of shapes was the transonic maneuver wing sections with reduced trailing edge deflections at the two most inboard stations. The sections have a common wing box shape, so that their combination results in geometry changes only where device deflection occurs. Requiring only six design variables to modify five span stations and the angle of attack, the shape approach is much simpler than the camber approach.

The design variables of the camber approach provide the capability to evaluate more complex camber shapes. The best mathematical representation of the variable camber devices is that which simulates the mechanical system being considered. Such an application is reported in Reference [23]. In principle, all possible wing section shapes that the mechanical system can provide are included in the "design space" the optimization process searches. The numerical optimization could be used to compare the best aerodynamics available for each of several mechanical systems. The baseline configuration did not define a mechanism for its variable camber system. The numerical model used for this study was considered representative of a simple, general, variable camber mechanical system.

The second set of design variables provides the advantage of simplicity. As the design variables vary, it is easier to visualize the corresponding wing geometry. The aerodynamics of the gradient information (i.e., the effect of design variable perturbations) obtained during the optimization process can be easily interpreted by the user. Thus the "aerodynamic systems" being considered by the designer are evaluated. With fewer design variables, the numerical optimization searches a smaller design space. This reduces the necessary computer time, but may restrict the design space to a region that does not include the "true" optimum. The user need choose wing section shapes that provide the optimization process a geometry that will meet the design requirements. The success of the numerical optimization is always dependent on the aerodynamic perception of the user, especially as the number of design variables is reduced.

4. TRANSONIC PERFORMANCE OPTIMIZATION

Initial results using the camber approach with twelve design variables produced a calculated drag reduction of more than thirty counts (for the inviscid, thinned-grid analysis). This was obtained with two PANDORA runs, each with two optimization iterations. The second run was started with the design variable values from the end of the first run, but the optimization history was not saved for starting the second run. Total CPU time was less than two hours. The changes in spanwise distribution of lift and drag are shown in Figure 17. The design "moved" quickly to the lower limit of the tolerance on the lift constraint (i.e., the lift was slightly below the constraint value). The pitching moment constraint was inadvertently specified such that it was violated at the start of the optimization. The optimization results increased the pitching moment by more than .01 to satisfy the constraint. The constraint value was not changes since the less negative pitching moment would reduce trim drag and the numerical optimization was apparently not penalized significantly.

The optimization runs with sixteen design variables (see Section 4.3) were started with the results of the first two runs. The extra design variables for the tip and root regions were run separately. Each run had two optimization iterations. No significant drag reductions were obtained. To further evaluate this approach, three additional runs were made with sixteen design variables (the extra design variables were used in the root region). Two of these runs redefined the optimization criteria. This changes the optimization search directions so that different regions of the design space are explored. One run sought to minimize the square root of the drag, while the other sought to maximize the lift, with a drag constraint of not more than the starting value. The starting geometry was the result of the first two runs. No significant design variable changes occurred. Two optimization iterations were done for the lift maximization and one optimization iteration was done for the square root of drag minimization. It is interesting to note that the initial search direction did differ significantly between these additional runs and the basic drag minimization run.

The third run perturbed the starting values of the design variables. The perturbation raised the trailing edge at the two most inboard span stations. The rest of the device geometry was that at the end of the first two optimization runs. The drag was to be minimized with lift and moment constrained. The gradient information from the previous runs was used to calculate starting values that would satisfy the constraints but increase the drag. In one optimization iteration the drag was reduced more than fifty counts, but the design variables that were manually changed at the start did not return to their previous values. The resulting design variable values were used to start a run with two optimization iterations. No significant change occurred.

The final results of all the optimization runs with the camber approach was a predicted drag reduction of more than forty counts, ignoring any changes in lift and moment (approximately -.01 and +.01, respectively). Total CPU time for all the optimization runs was less than four hours. The trailing edge location at span stations 0.544 and 0.816 moved downward, whle that of the theoretical tip moved upward. A "full-grid" wing-body viscous analysis at the nominal design conditions shows the lift coefficient to be approximately .04 less than the starting value. Matching the starting lift value, the estimated drag reduction was less than six counts. With the trim drag reduction due to less negative pitching moment, the total expected drag reduction was approximately fifteen counts.

The second optimization approach used significantly less computer time because of the fewer number of design variables. Two runs, each with three optimization iterations, reduced the predicted drag value by more than twenty counts. Again, the starting solution violated the pitching moment constraint and the lift was reduced to the lower limit of its constraint value. Essentially all of the drag reduction occurred during the first run. A third run to minimize the square root of the drag produced no significant changes in two optimization iterations. Total CPU time was less than two hours.

Relative to the baseline transonic maneuver geometry, the predicted drag reduction for the shape approach was essentially the same as the camber approach (more than forty counts). Changes in lift and moment were also the same. The trailing edge location of the two most inboard devices was raised, while that of the third (span station .544) was lowered. The leading edge was moved downward at all three outboard span stations. Again, a "full-grid", viscous, wing-body analysis indicated a drag reduction of less than six counts at the starting value of lift. With the expected trim drag change, the total drag reduction was again approximately fifteen counts.

The problem of local and global optimums in an optimization problem was demonstrated by the results of the two approaches. The two "optimum" device deflections moved in opposite directions at span stations .544 and 1.0. The predicted performance is the same, which may or may not be the "true" optimum. There is little doubt of the non-uniqueness of a configuration design problem. The design space must include the true optimum if it is to be found with numerical optimization. If several optimums exist, then several different design

variables or different starting solutions are needed to find the other optimums. If a local optimum meets the performance goals of the design problem, then the search for other optimums may be academic.

5. WIND TUNNEL TEST

The two wing geometries designed with the PANDORA code were tested in the Arnold Engineering Development Center 16T Propulsion Wind Tunnel in April 1980 [24]. The CDAF configuration had been tested previously in the 16T tunnel in April and November 1979 [25,26]. For all tests, the Reynolds number was 3.0 million per foot for subsonic Mach numbers. The fifteenth scale model had a mean aerodynamic chord of 11.3 inches, and was instrumented with a six component balance. Ninety six pressure taps were distributed on five wing span stations and two canard span stations. The wind tunnel model is shown in Figure 18. The April 1980 test included canard on and off and nacelle on and off pressure data to provide a data base for both current and future code verification.

An "alternate maneuver" wing geometry was tested in November 1979. The alternate geometry represents a variable camber shape between the transonic cruise and original transonic maneuver. The model parts for the alternate maneuver geometry were made from the original transonic maneuver model parts. Thus, the baseline geometry used to start the optimization was not avaialble for the test in April. The alternate transonic maneuver geometry was tested with the PANDORA developed geometries to provide a test repeat reference.

SECTION V

AERO DATA EVALUATION

Data for the three tested configurations at Mach 0.9 are summarized in Figures 19-21. The wing-body pitching moment non-linearities indicate strong wing tip flow separation. This was confirmed by oil flow visualizations. Wing-body-canard data are included in the figures. Again the pitching moment non-linearities indicate strong viscous effects: wing tip separation and vortex flow on the canard.

In addition to flow separation, the flow near the wing tip is quite severe for potential flow analysis (e.g., Figure 9). Data show local Mach numbers in excess of 1.7. The limit of potential flow analysis is generally considered to be about Mach number 1.3. A more complete flow equation (e.g., Euler, Navier-Stokes) need be used to accurately predict the flow details.

Figure 22 is a comparison of the April 1980 and November 1979 test data for the alternate maneuver configuration. Significant differences are seen. The April data show more negative zero-lift pitching moment, more negative zero-lift angle of attack and less drag at all lifts. Flow angularity is the suspected cause. A model support problem required different model positioning in the tunnel, although the April test position should be identical to the November position at seven degrees angle of attack. Flow angularity corrections used in the data reduction were the same as for the previous tests. The model support prevented running the model inverted to check the flow angularity during the April test.

Test results for wing-body lift and drag are compared to each other and code predictions in Figure 23. Code predictions are good. The code does not model the vertical tail which is present in the data. Ten counts of drag have been added to the analysis results. The predicted drag levels agree with the data within twenty-five counts. The data show that the two PANDORA shapes have essentially the same performance as predicted by the optimizaton runs.

Lift and drag data and predictions for wing-body-canard configurations are shown in Figure 24. The relative performance of the three tested configurations is the same as in Figure 23. Code predictions are within twenty-five counts of the data. Again, the vertical tail is included in the data, but not the analysis. Thirty counts of drag have been added to the analysis results.

Earlier tests measured the zero-lift drag increment of the vertical tail as ten counts, the same as the drag increment added to the wing-body predictions of Figure 23. However, thirty counts have been added to the predicted wing-body-canard drag predictions. This different drag increment is apparently due to the different grids used for wing-body and wing-body-canard analysis. (An input option in the code will provide wing or wing-body analysis in a wing-canard or wing-body-canard grid.) For comparison of the relative performance of different wing geometries (analyzed with the same grid), this drag increment is not significant. The relative performance of geometry changes is what is used by the numerical optimization. Waggoner [27] used the base code of Reference [1] to evaluate planform modifications of a supercritical wing. His results show that the predicted incremental changes in force and moment can be used as a design guide to compare similar configurations. A twenty count drag difference could be due to a normal force coefficient difference of 0.02 at seven degrees angle of attack (four percent of the nominal lift coefficient of 0.5). This suggests that the grid effect in these results represents different levels of convergence of the lift.

The lack of "complete" lift convergence generally results in the underprediction of the lift for a given angle of attack (the code underpredicts the lift curve slope). For a given lift value, the angle of attack for the code is greater than that for the data and the difference increases as the lift increases. Thus the code results show more drag increase with lift (i.e., a less efficient drag polar) than the data. If the normal and axial force are calculated from the code results, and then lift and drag values were calculated at the "corrected" angle of attack, the predicted drag polar efficiency would increase. For example, an 0.5 angle of attack correction results in a drag change of 17 counts at C_L = 0.2, 44 counts at C_L = 0.5, and 61 counts at C_L = 0.7. The "error" in the angle of attack for the code is actually an underprediction of the lift. The development of lift within the code is very slow. Faster solution methods (e.g., References [28,29]) would relieve this problem.

The predicted force and moment changes due to candard incidence changes are compared to data in Figures 25 and 26. The predicted drag changes, longitudinal stability level and moment change due to canard incidence show good agreement with the data. As for the previous wing-body-canard predictions, thirty counts of drag have been added to the code results. For the pitching moment predictions, an increment of +.030 for the supersonic cruise geometry and +.055 for the alternate maneuver geometry have been added to the code results.

Part of the pitching moment increment can be interpreted as an error in the zero lift pitching moment. This error is approximately the same as the examples shown in Reference [1]. The apparent causes of this error are the body contributions to moment, the boundary layer effects on the aft loading of the wing section and the underprediction of the leading edge peak pressures.

The body solution develops only through the global crude grid. This provides the major influence of the wing/body and canard/body interaction, but neglects details at the body surface, in particular at the nose of the body. The boundary layer effects on the pitching moment are indicated in the pressures in Figure 9. the most inboard span station shows the predicted pitching moment is more negative. The boundary layer influence on shock position is also important. Empirical formulas are used to model boundary layer separation [1]. No explicit treatment of shock-boundary layer interaction is provided in the code. The underprediction of leading edge peak pressures would also cause a more negative pitching moment prediction. A denser grid point distribution at the leading edge would improve this.

The results for the mildly cambered supersonic cruise geometry indicate the magnitude of the body and leading edge pressure pitching moment error (ΔC_m = +.030). The results for the more highly cambered, highly loaded alternate maneuver geometry indicate the additional error due to the viscous effects (ΔC_m = +.055 vs. +.030). The pitching moment error precludes predicting actual trim conditions, but does not significantly impact the pitching moment gradient information used for numerical optimization.

SECTION VI

EVALUATION OF DESIGNS

The application of the design methodology to the CDAF configuration took approximately four hours of CDC 7600 CPU time for the camber approach and less than three hours CPU time for the shape approach. Nearly all of the geometry changes occurred in the first two optimization runs, using approximately two hours of CPU time for each approach. Calendar time for the two methodology applications was approximately one month. Test results showed the resulting performance improvement to be a drag reduction of fifteen counts.

Thus, one design methodology application would use approximately two hours of CPU time and two weeks of calendar time (for an approach that has no non-transonic performance penalties). Four hours of CPU time would be adequate for a general, multi-point design application.

The benefits of using the design methodology can be evaluated by comparison with a "manual" design approach. A manual approach would be one that uses an empirical design methodology based on experimental experience with similar configurations. The computational tools used may include 3-D subsonic and 2-D transonic codes. At some point, the manual approach need be "calibrated" with wind tunnel data if it is to provide a quantified performance estimate. Without its own experimental verification, the performance of a new wing design can only be estimated based on previously tested configurations.

The above comparison allows a large range of claims about the design methodology benefits. A detailed, quantified cost comparison can not be made since labor, testing and computer costs vary substantially. Ignoring calendar time, the only significant cost of the automated design methodology is the computer resources. The cost of the manual approach need include some of the expense of acquiring the experimental data that developed the empirical design methodology for the configuration type. If test results for the original design do not achieve the performance requirements, additional wind tunnel testing of a new geometry is needed to quantify any performance improvement. A manual approach can never conclude that a geometry is optimum with additional testing. Such a conclusion is the end result of numerical optimization. The automated design methodology provides its own baseline performance "data" and quantifies the expected performance improvements.

The cost of fabricating and testing one additional wing geometry is twenty to forty thousand dollars. The lower number is more than the cost of four hours of CDC 7600 computer time. If the code results can be used to eliminate the need to test an additional wing geometry, then the cost savings equal, or exceed, the computer costs. If the original wind tunnel test indicates a design deficiency, the manual design approach also requires the time between the original and subsequent wind tunnel tests. It is clear that the automated design methodology can provide development time or costs for the design of advanced fighter configurations.

The potential flow transonic analysis limited the design point lift to a value below the actual maneuver design point. A manual approach has no such limitation because it uses wind tunnel data. The ability of the automated design procedure to produce a performance improvement was demonstrated by the measured drag reduction at the optimization design lift. The crucial requirement to obtain a significant impact on the mission performance is the ability of the transonic analysis to accurately analyze the design point conditions.

A drag reduction of fifteen counts is very small compared to the total drag at transonic maneuver conditions. In fact, a thirty count drag reduction was felt to be the minimum for a "significant" impact on the configuration. However, if the computational analysis can be used to confidently predict that a given wing geometry is the "optimum," then considerable design time and costs can be saved. Several CPU hours is a small expense compared to that of the design, fabrication, and test of an additional set of wing devices. As improvements in both computer and code capability continue to be made, numerical methods become more cost effective. If existing faster computers are considered, CPU time reductions of a factor of two to five are obtainable. Such a reduction would allow more accurate analysis (e.g., explicit viscous effects, greater density grids) and yet use considerably less CPU time than that reported here.

This study was limited to one particular design application for a supersonic cruise transonic fighter. As discussed in previous sections, the final design problem for numerical optimization was a small part of the complete configuration design problem. Approximations made during the design problem numerical modeling (e.g., trim drag benefits, viscous effects) reduced the measured performance improvements from that predicted by the optimization runs. The benefits of numerical optimization will increase as the accuracy and completeness of the numerical simulation of the design problem increases.

SECTION VII

FINAL DESIGN PROCEDURE

The experience of applying the original design procedure to the CDAF configuration led to several conclusions regarding the design methodology application. The design methodology is most effective when the numerical optimization is used most efficiently. Two key items can be identified for this: definition of the optimization function and design variables; and adequate analysis code accuracy.

All of the significant performance improvements occurred in the first two optimization iterations. The additional runs which made slight changes in the optimization function were not worthwhile. Changing the starting geometry or the design variables is more effective. Minimizing the drag or its square root (with a lift constraint) are the same optimization problem. Maximizing the lift-to-drag ratio with a lift constraint is probably better.

During the optimization, the influence of the design variables is calculated for the gradient information. When identified, the less effective design variables should be eliminated. The use of wing section shapes can produce good results with relatively few design variables. Detailed geometry variations with the numerical optimization is appropriate when specific local aerodynamic characteristics need be modified. If a mechanical system is to be modeled, then the design variables may be pre-determined by the system mechanism or else be sufficiently detailed to simulate a proposed system. Such a case is as much an optimization of the mechanical system as it is the configuration aerodynamics.

The need for accurate transonic analysis in the numerical optimization is clear. Inaccuracies in the analysis produce errors in the gradient information used in the optimization search. Reduced mesh densities reduce the necessary computer time, but at the risk of unacceptable analysis errors. Each design application should evaluate the impact of reduced mesh densities with several code analysis runs. Although fifty streamwise points per airfoil chord were used for the CDAF design, eighty points per chord seem necessary. The spanwise reduction of the fine grid system (from fifteen stations on the exposed span to twelve) yields satisfactory results. Improvements in the analysis code efficiency would reduce the necessary computer time without any decrease in the analysis accuracy. More advanced computers and solution algorithms will improve the computer time/accuracy trade off. For example, the analysis code in PANDORA has been made twenty percent more efficient in CPU time since the original design methodology application.

The numerical optimization had no difficulty in making large performance improvements to a "bad" starting geometry. During the CDAF design application, the starting design variables were altered to degrade the performance by approximately 50 counts of drag. This drag penalty was completely eliminated in one optimization iteration.

As a demonstration of the final design procedure, three optimization runs were made to increase the lift-to-drag ratio of the CDAF configuration. The values of lift and moment calculated for the alternate maneuver geometry at seven degrees angle of attack were design constraints. The integrated force and moment on the exposed wing planform for an inviscid, wing-body analysis were the parameters used in the optimization. The shape approach was used with five design variables combining the alternate maneuver and transonic cruise wing section geometries (and varying the angle of attack). The three optimization runs had different starting conditions: the first was the alternate maneuver geometry at seven degrees angle of attack, the second was the transonic cruise geometry at eight degrees angle of attack and the third was the transonic cruise geometry at nine degrees angle of attack. The results are shown in Figure 27, and discussed below.

Very little drag reduction (approximately six counts) occurred when the optimization was started with the alternate maneuver geometry. Two optimization iterations required 0.6 hours of CPU time. The transonic cruise geometry at eight degrees angle of attack violates the lift constraint. The optimization algorithm first seeks to satisfy the violated constraint with the least performance penalty. This results in a drag level of 617 counts at C_L = .558. The next optimization iteration moves to C_D = .0603, C_L = .568 and then the third iteration results in C_D = .0594, C_L = .572. Four additional iterations were run, with the final result being C_D = .0542, C_L = .558. The drag level for the starting transonic cruise geometry at C_L = .558 would be 665 counts. Thus, the six optimization iterations reduced the drag level by more than 120 counts at the required lift. Total CPU time was approximately 1.6 hours. This result is slightly better (six counts) than that for starting with the alternate maneuver geometry, although four additional optimization iterations were necessary.

The third optimization run started with the transonic maneuver geometry at a lift greater than that required (C_L = .567, C_D = .0700). It is interesting to note that for this run the first optimization iteration results in nearly the same point as the third iteration of the run which began with the lift constraint violated. The optimization results for the two runs behave the same from that point on. The optimization run which started with the lift constraint satisfied would require at least two fewer optimization iterations than the run which started with the lift constraint violated. Total CPU time for the third optimization run was 0.5 hours.

The major conclusion from these results is that the most efficient application of the numerical optimization occurs when the design is started nearest to its optimum. Making the optimization algorithm do the work of satisfying the constraints or making large changes in the geometry uses computer time unnecessarily. Although large improvements in the performance may provide a greater

sense of satisfaction, the performance of the final geometry is the true measure of success. It is clear that the design methodology will be more cost effective if only two optimization iterations, rather than six, are used to produce the same performance.

Wider use of numerical optimization is impeded by the large amount of computer time that it requires. Thus, the incorporation of faster solution algorithms in the analysis code is the most important next development. The result of faster solution algorithms operating on newer, faster computers may be more than a factor of ten reduction in the CPU times reported here. This will allow substantial reductions in the computer time while improving the solution accuracy. Additional improvements to the solution accuracy would come from a more accurate wake model and a more accurate boundary layer calculation. With the trim surface included in the aerodynamic analysis, the ability to accurately predict trimmed flight conditions should be pursued.

SECTION VIII

CONCLUSIONS

The results described here show both the benefits and hazards of numerical optimization for aerodynamic design. The numerical optimization will work best when both the flow field analysis and numerical model of the design problem are accurate. Although greater computer resources are generally needed for more complex and accurate analysis, the cost of numerical optimization would still be less than that of additional wind tunnel testing. As both computer and analysis code capability increase, numerical optimization will take a greater role in aerodynamic design. The key elements for efficient numerical optimization are to use relatively few design variables and to start the optimzation as close as possible to the desired performance goal.

For a variable camber wing geometry, evaluation of different mechanical systems is well suited for numerical optimization. Numerical optimization can be used to evaluate the resulting performance of mechanical systems with different complexity, cost or weight. The aerodynamic designer can best use numerical optimization by running two or three iterations for a variety of geometries and starting conditions. The numerical optimization will conduct a systematic parametric evaluation using the flowfield analysis as if it were a wind tunnel. The computer can be used to compare many different configurations over several days time at a small fraction of the time and cost that would be needed to conduct a wind tunnel test.

Wider use of transonic numerical optimization will occur when the necessary computer time is reduced and the analysis accuracy is increased. Incorporation of faster solution algorithms will make the largest contribution towards this goal. Everday use of numerical optimization for aircraft design will occur when the code can provide an efficient, accurate prediction of minimum trimmed drag for transonic flight.

REFERENCES

1. "Configuration Development of Advanced Fighters," Final Technical Report, AFWAL-TR-80-3142, November 1980.

2. Riccioni, E. E.; and Draper, A. C. (Conference Chairman): "Design Conference Proceedings: Technology for Supersonic Cruise Military Aircraft, Vol. 1" (U), AFFDL-TR-77-85, April 1976. (Unclassified)

3. Boppe, C. W.: "Transonic Flowfield Analysis for Wing-Fuselage Configurations," NASA Contractor Report 3243, May 1980.

4. Boppe, C. W.: "Calculations of Transonic Wing Flows by Grid Embedding," AIAA Paper 77-207, January 1977.

5. Boppe, C. W.: "Computational Transonic Flow About Realistic Aircraft Configurations," AIAA Paper 78-104, January 1978.

6. Boppe, C. W. and Stern, M. A.: "Simulated Transonic Flows for Aircraft with Nacelles, Pylons and Winglets," AIAA Paper 80-130, January 1980.

7. Boppe, C. W., and Aidala, P. V.: "Complex Configuration Analysis at Transonic Speeds," in Subsonic/Transonic Configuration Aerodynamics, AGARD CP-285, September 1980.

8. Mason, W. H., et al.: "An Automated Procedure for Computing the Three-Dimensional Transonic Flow Over Wing-Body Combinations, Including Viscous Effects," AFFDL-TR-77-122, Vol. 1, October 1977.

9. Nash, J. F. and Tseng, R. R.: "The Three-Dimensional Turbulent Boundary Layer on an Infinite Yawed Wing," The Aeronautical Quarterly, November 1971.

10. Bradshaw, P. and Ferriss, D. H.: "Calculation of Boundary Layer Development Using the Turbulent Energy Equation. Compressible Flow on Adiabatic Walls," J. Fluid Mech., Vol. 46, 1971.

11. Hinson, B. L. and Burdges, K. P.: "Acquisition and Application of Transonic Wing and Far-Field Test Data for Three-Dimensional Computational Method Evaluation," Technical Report, AFOSR-TR-80-0421, March 1980.

12. Vanderplaats, G. N.: "COPES-FORTRAN Control Program for Engineering Synthesis," to be published as a Naval Postgraduate School Memorandum.

13. Vanderplaats, G. N." "CONMIN--A Fortran Program for Constrained Function Minimization," NASA TM X-62282, August 1973.

14. Vanderplaats, G. N., Hick, R. M. and Murman, E. M.: "Applications of Numerical Optimization Techniques to Airfoil Design," NASA SP-347, Part II, 1975.

15. Vanderplaats, G. N. and Hicks, R. M.: "Numerical Airfoil Optimization Using a Reduced Number of Design Coordinates" NASA TM X-73151, 1976.

16. Woodward, F. A., et. al.: "Analysis and Design of Supersonic-Wing-Body Combinations, Including Flow Properties in the Near Field," NASA CR-73106, 1967.

17. Harris, R. V.: "An Analysis and Correlation of Aircraft Wave Drag" NASA TM X-947, 1964.

18. Boppe, C. W.: "A Computer Program for Calculating Subsonic Aerodynamics of Complex Wing-Body Configurations (A User's Guide)," Grumman Aerodynamics Technical Report No. 393-73-1, October 1973.

19. Mason, W. H.: "Computation of Minimum Trimmed Drag Attainable on Complex Configurations and the Associated Design Spanloads," Grumman Memorandum EG-ARDYN-78-44, May 1978.

20. Meyer, R. C., Fields, W. D.: "Configuration Development of a Supersonic Strike-Fighter," AIAA Paper 78-148, AIAA 16th Aerospace Sciences Meeting, Huntsville, Alabama, January 1978.

21. Hendrickson, R., Grossman, R., Sclafani, A. S.: "Design Evolution of a Supersonic Cruise Strike Fighter," AIAA Paper 78-1452, AIAA Aircraft Systems and Technology Conference, Los Angeles, California, August 1978.

22. Woodward, F. A.,: "An Improved Method for the Aerodynamic Analysis of Wing-Body-Tail Configurations in Subsonic and Supersonic Flow," NASA CR-2228, 1973.

23. Waggoner, E. G., Haney, H. P., and Ballhaus, W. F.: "Computational Wing Optimization and Comparisons With Experiment for a Semi-Span Wing Model," NASA TM 78480, 1978.

24. Spurlin, C. J.: Test Report for AFWAL Optimal Transonic Configuration Fighter, Project No. P41T-G6, Test No. TF-570, April 1980.

25. Spurlin, C. J.: Test Report for AFFDL CDAF Configuration, Project No. P41T-B2, Test No. TF-534, April 1979.

26. MacLanahan, D. A., Jr.: Test Report for AFFDL Advanced Survivable Aircraft Configuration, Project No. P41T-E0, Test No. TF-555, December 1979.

27. Waggoner, E. G.: "Computational Transonic Analysis for a Supercritical Transport Wing-Body Configuration," AIAA Paper 80-129, January 1980.

28. Holst, T. L.: "Fast, Conservative Algorithm for Solving the Transonic Full-Potential Equation," AIAA J., Vol. 18, Dec. 1980, pp. 1431-1439.

29. Jameson, A.: "Acceleration of Transonic Potential Flow Calculations on Arbitrary Meshes by the Multiple Grid Method," AIAA Paper 79-1458, July 1979.

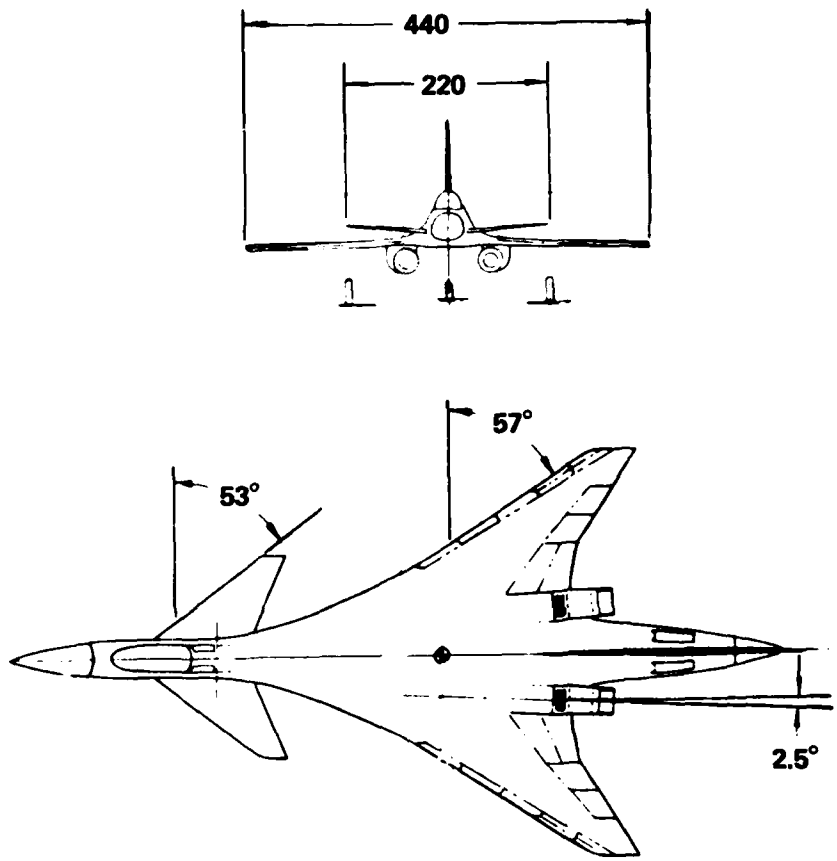

Figure 1. Fighter design configuration - CDAF preferred concept

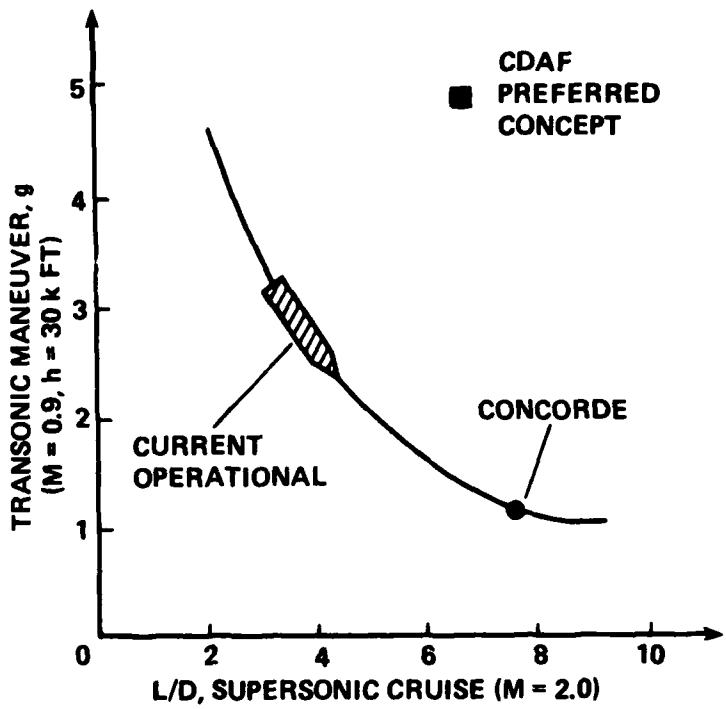

Figure 2. Comparison of transonic maneuver/supersonic cruise performance of current aircraft and the CDAF dual role concept

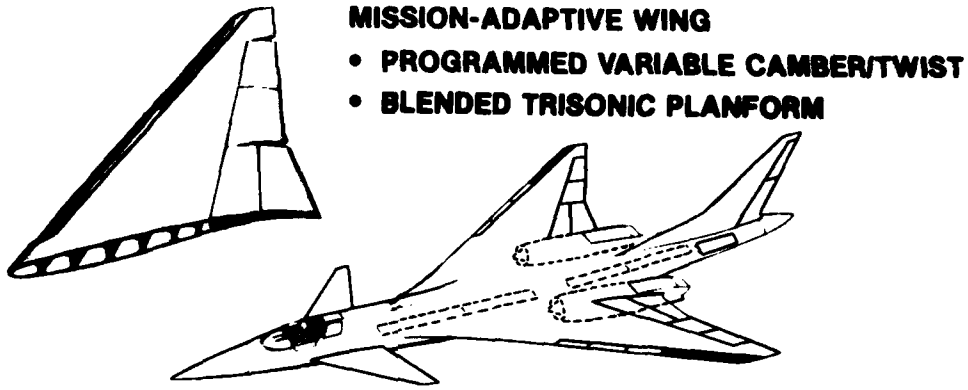

Figure 3a. Advanced technology implementation for the CDAF configuration - aerodynamics

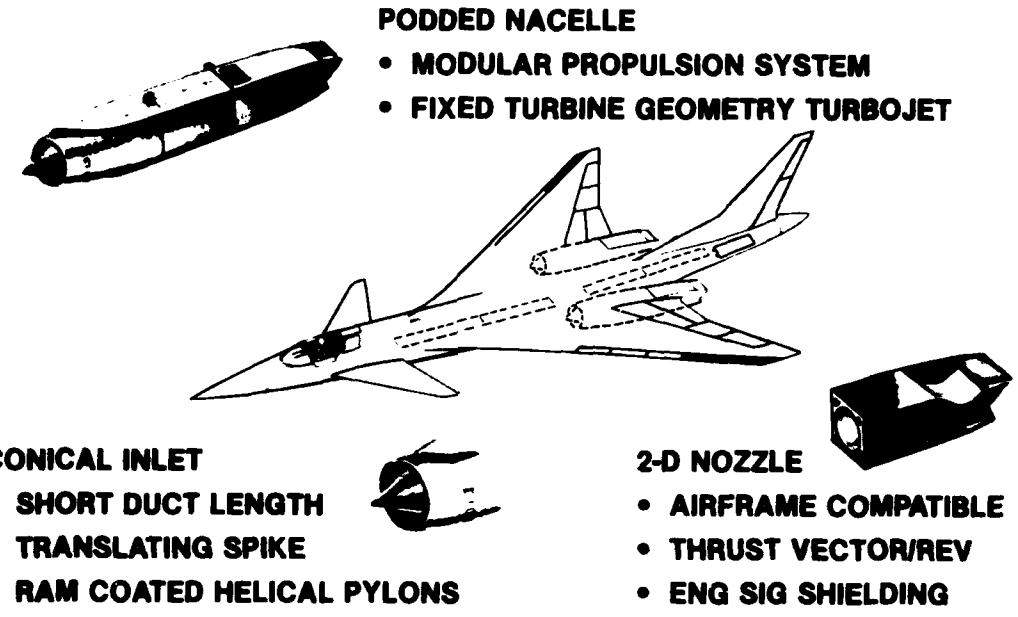

Figure 3b. Advanced technology implementation for the CDAF configuration - propulsion

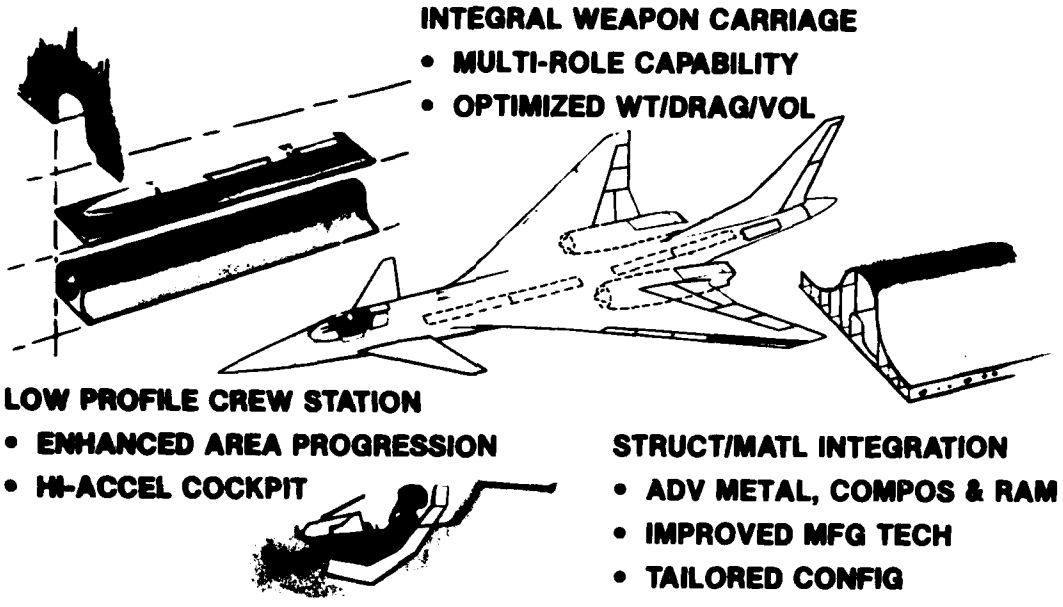

Figure 3c. Advanced technology implementation for the CDAF configuration - airframe

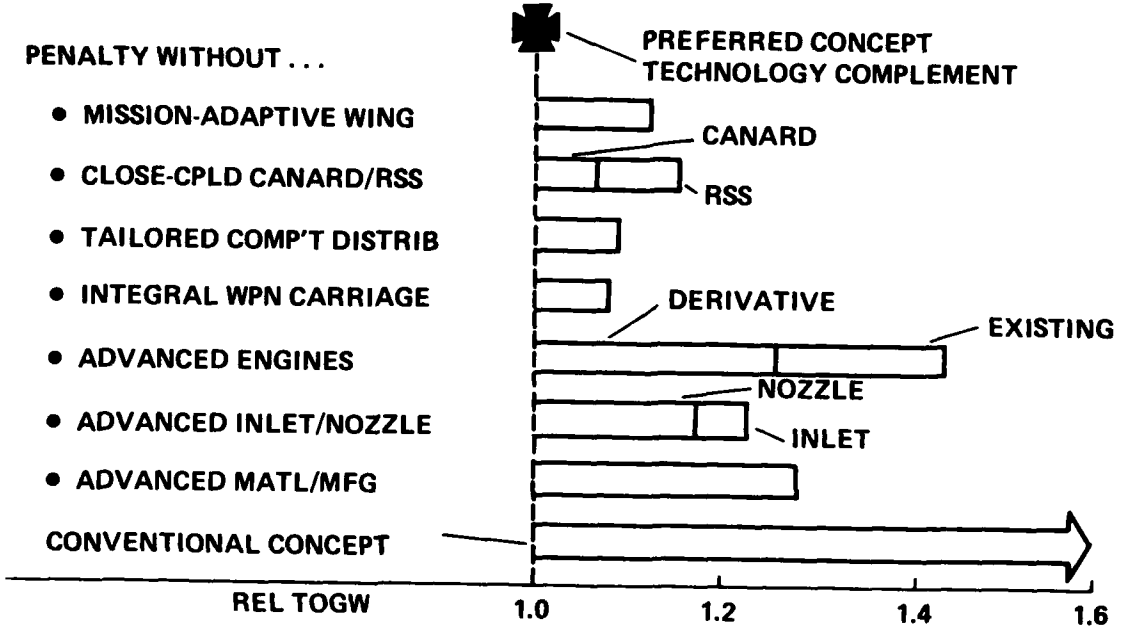

Figure 4. Advanced technology dependence of the CDAF configuration

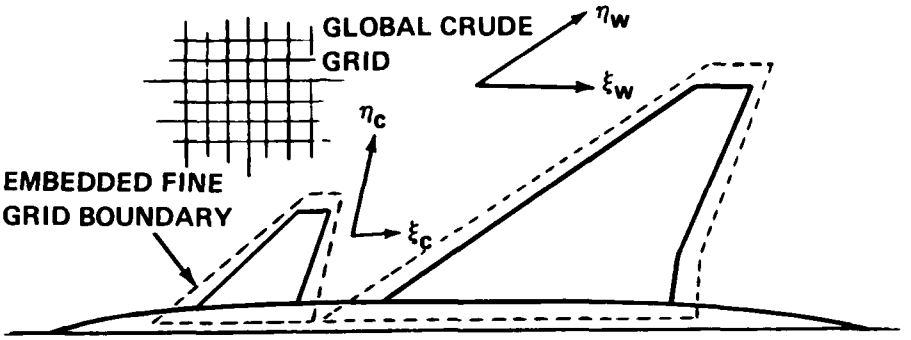

Figure 5. Embedded grid system for a wing-body-canard configuration

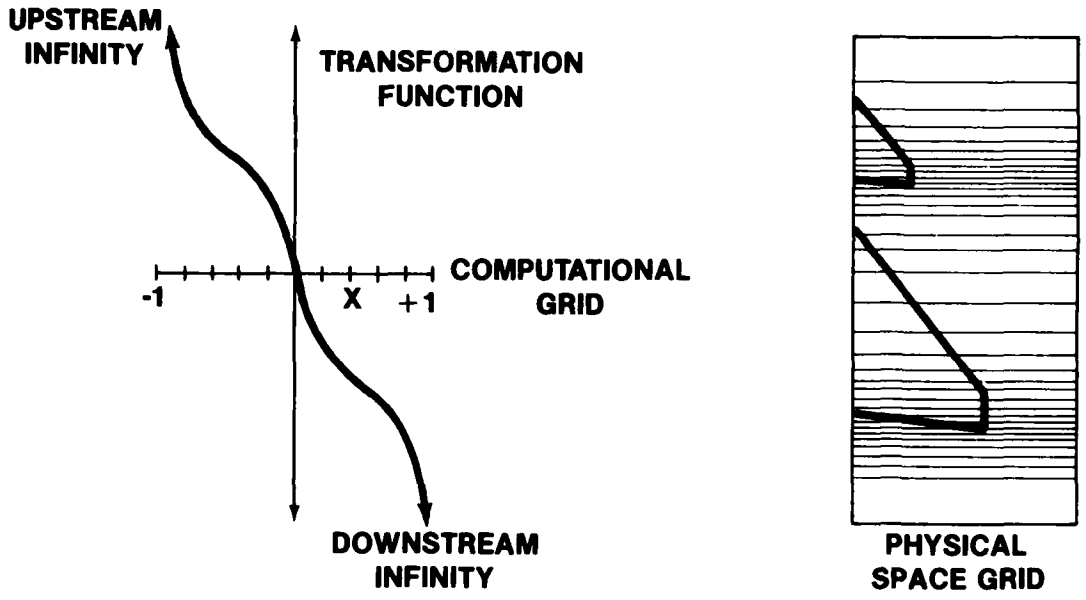

Figure 6. Grid transformation for wing-canard planforms

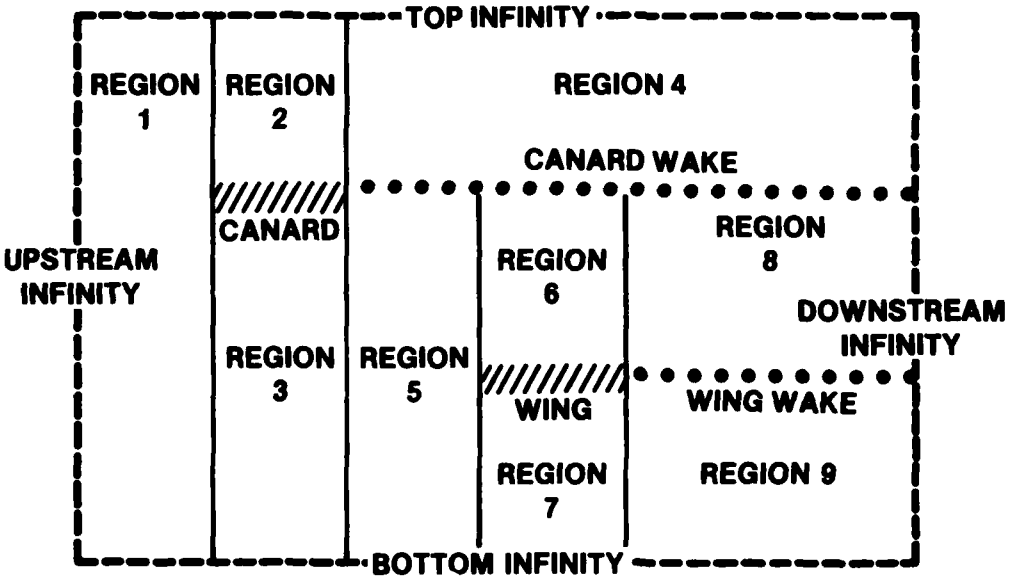

Figure 7. Vertical line relaxation region for multiple lifting surface analysis

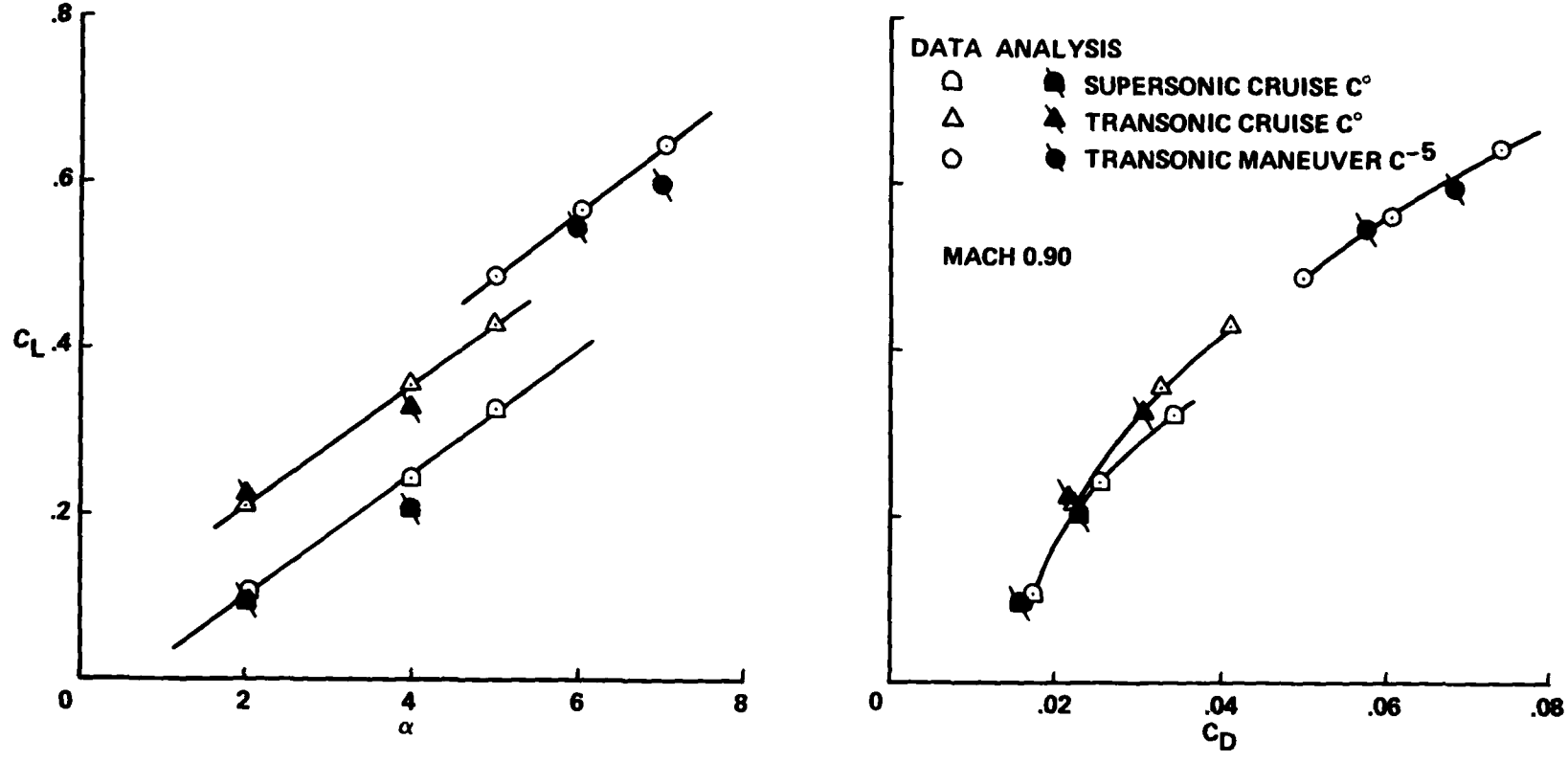

Figure 8. Wing-body-canard lift and drag, data-analysis comparisons, Mach 0.9

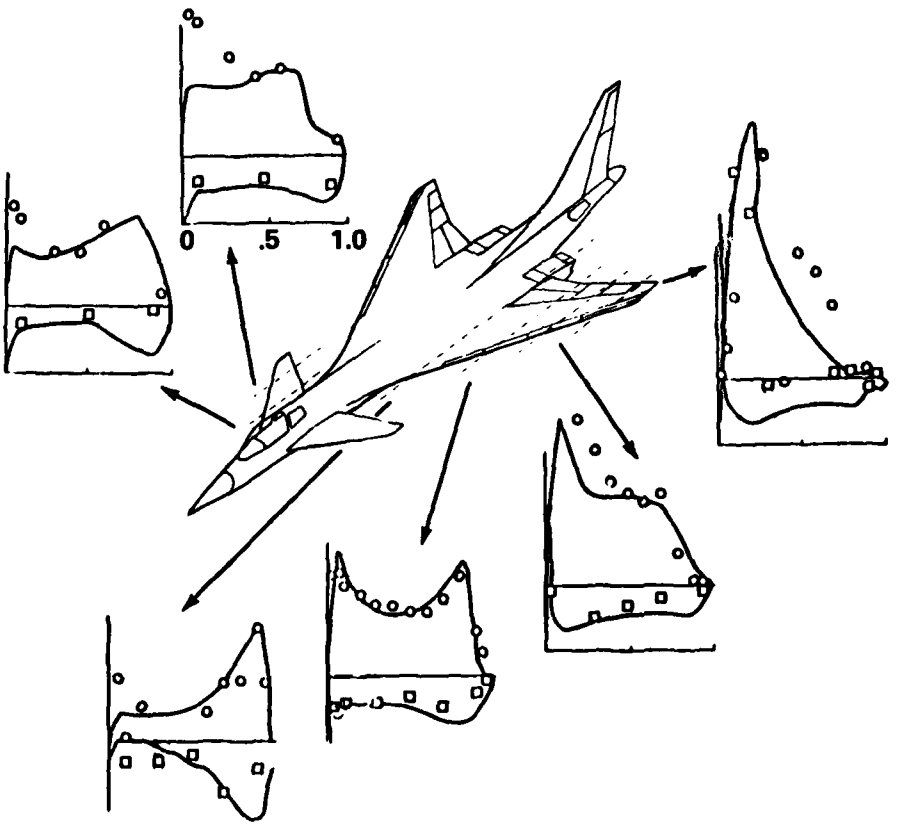

Figure 9. Wing-body-canard pressures, data-analysis comparison, Mach 0.9

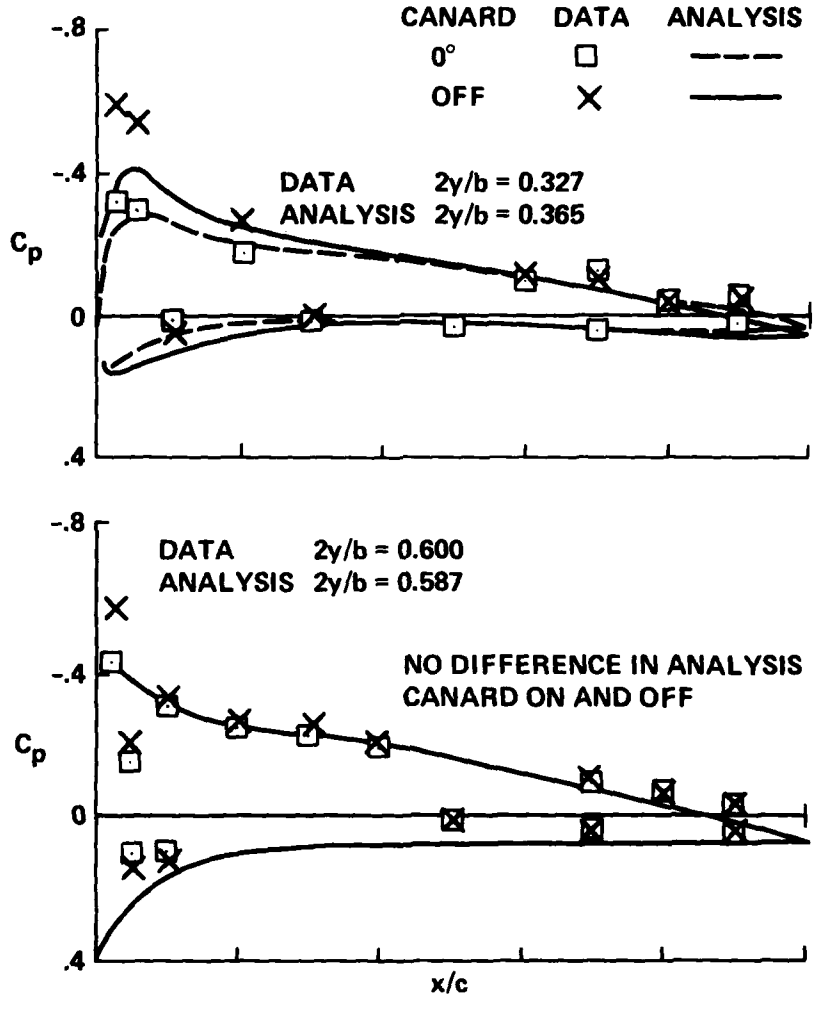

Figure 10. Wing pressure changes due to canard, data-analysis comparisons, Mach 0.9

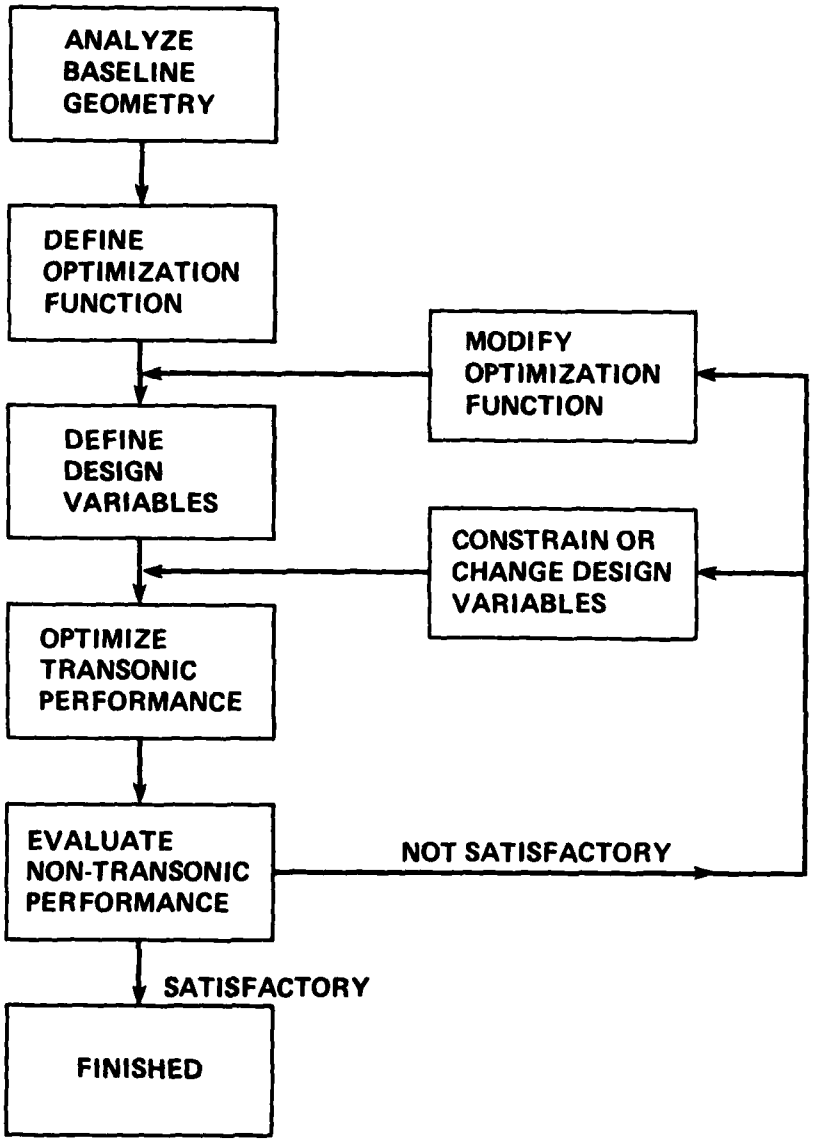

Figure 11. Design procedure outline

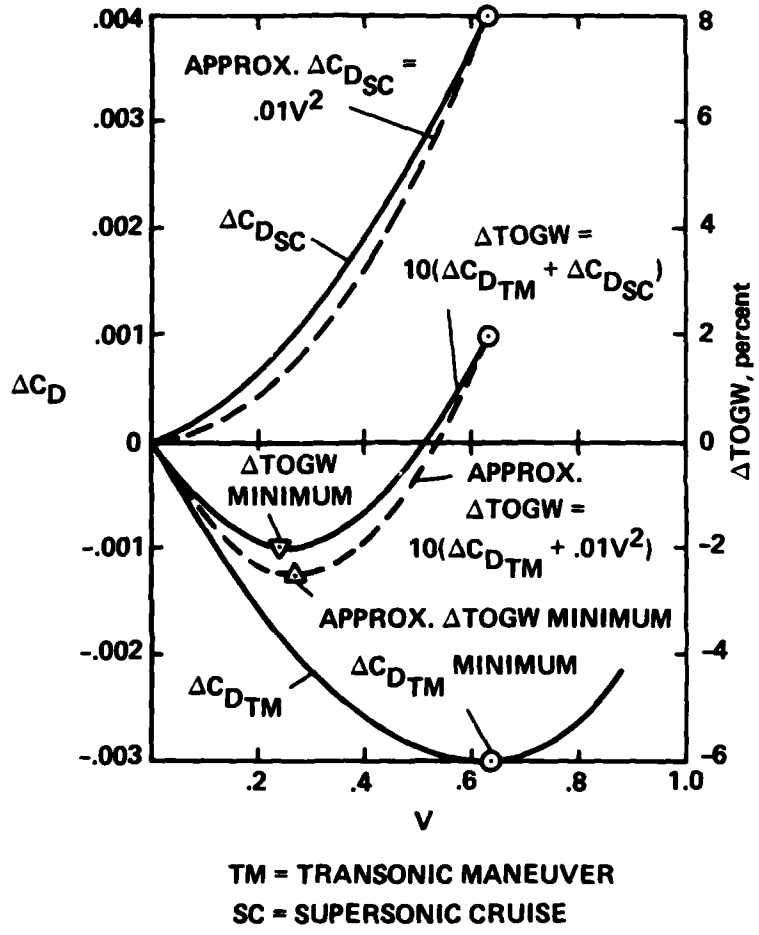

Figure 12a. Transonic optimization with supersonic cruise - supersonic drag penalty formula

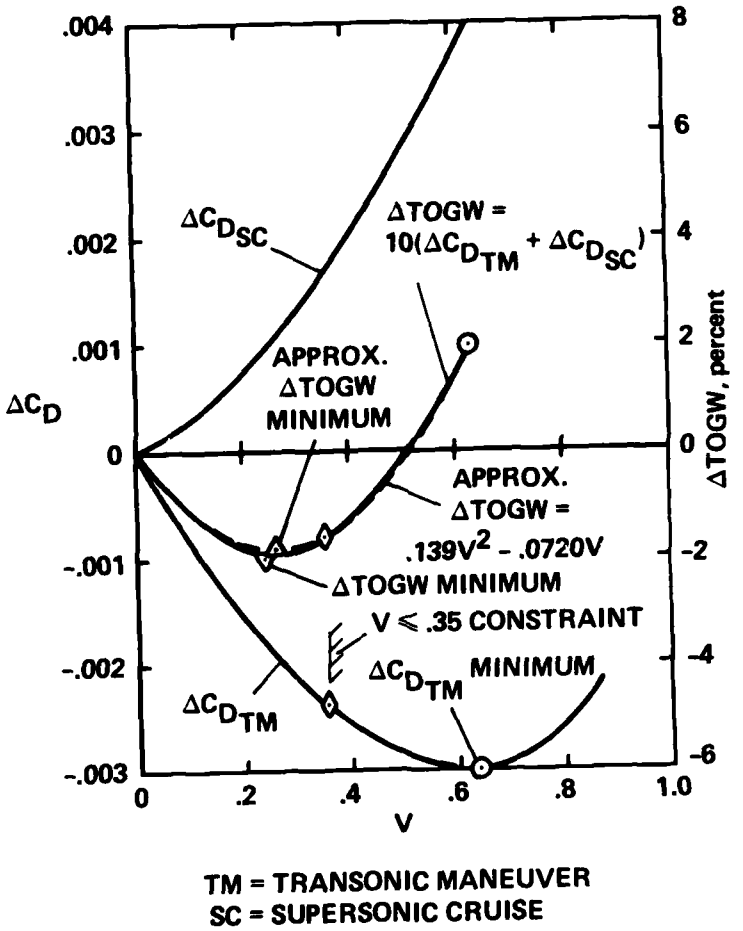

Figure 12b. Transonic optimization with supersonic cruise - design variable constraint method

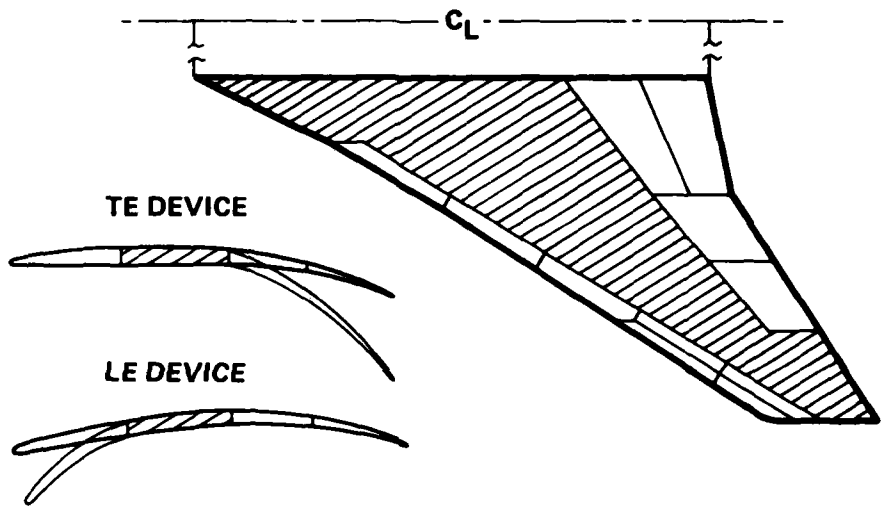

Figure 13. Variable camber segmentation for CDAF wing design

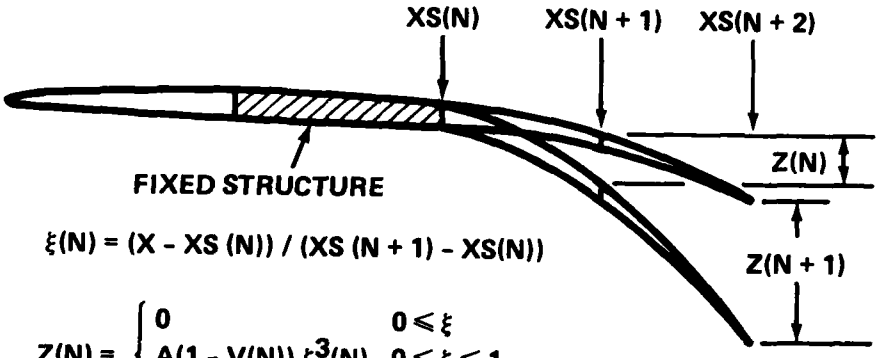

$$\xi(N) = (X - XS(N)) / (XS(N+1) - XS(N))$$

$$Z(N) = \begin{cases} 0 & 0 \leq \xi \\ A(1 - V(N))\,\xi^3(N) & 0 \leq \xi \leq 1 \\ B(1 - V(N))\,\xi\,(N) & 1 \leq \xi \end{cases}$$

WHERE

XS = CHORD STATION
Z = DEFLECTION
V = DESIGN VARIABLE
A,B = COEFFICIENTS FOR CONTOUR MATCHING

Figure 14. Camber Approach model for wing design optimization

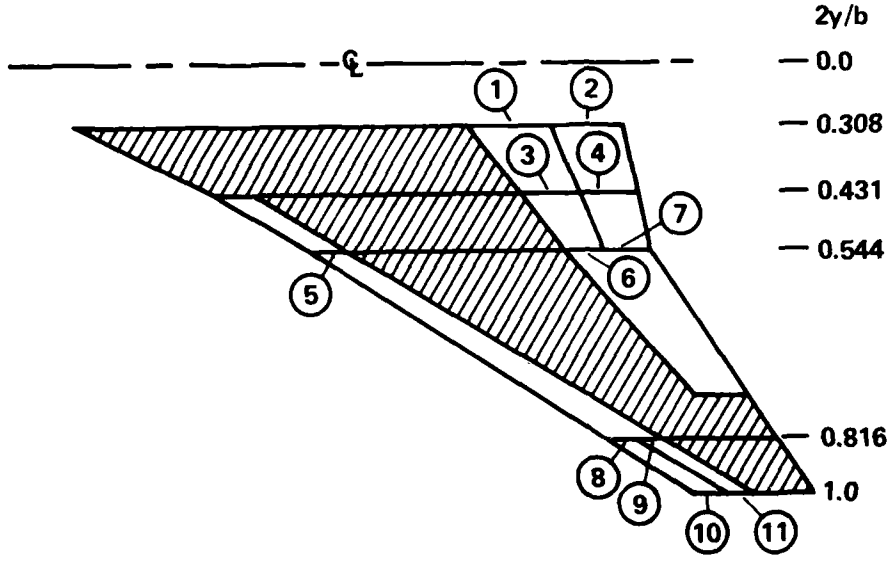

Figure 15. Camber approach design variable assignment

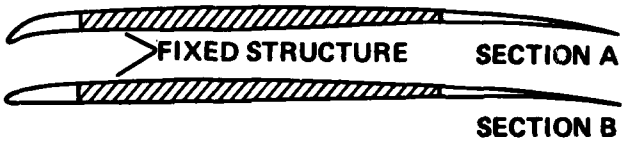

FOR WING SECTION N

$$Z(N) = ZA(N) \cdot (1-V(N)) + ZB(N) \cdot V(N)$$

WHERE

Z(N) = WING SECTION ORDINATES AT SPAN STATION N
ZA(N) = WING SECTION A ORDINATES FOR SPAN STATION N
ZB(N) = WING SECTION B ORDINATES FOR SPAN STATION N
V(N) = DESIGN VARIABLE FOR SPAN STATION N

Figure 16. Wing section shape model for wing design optimization

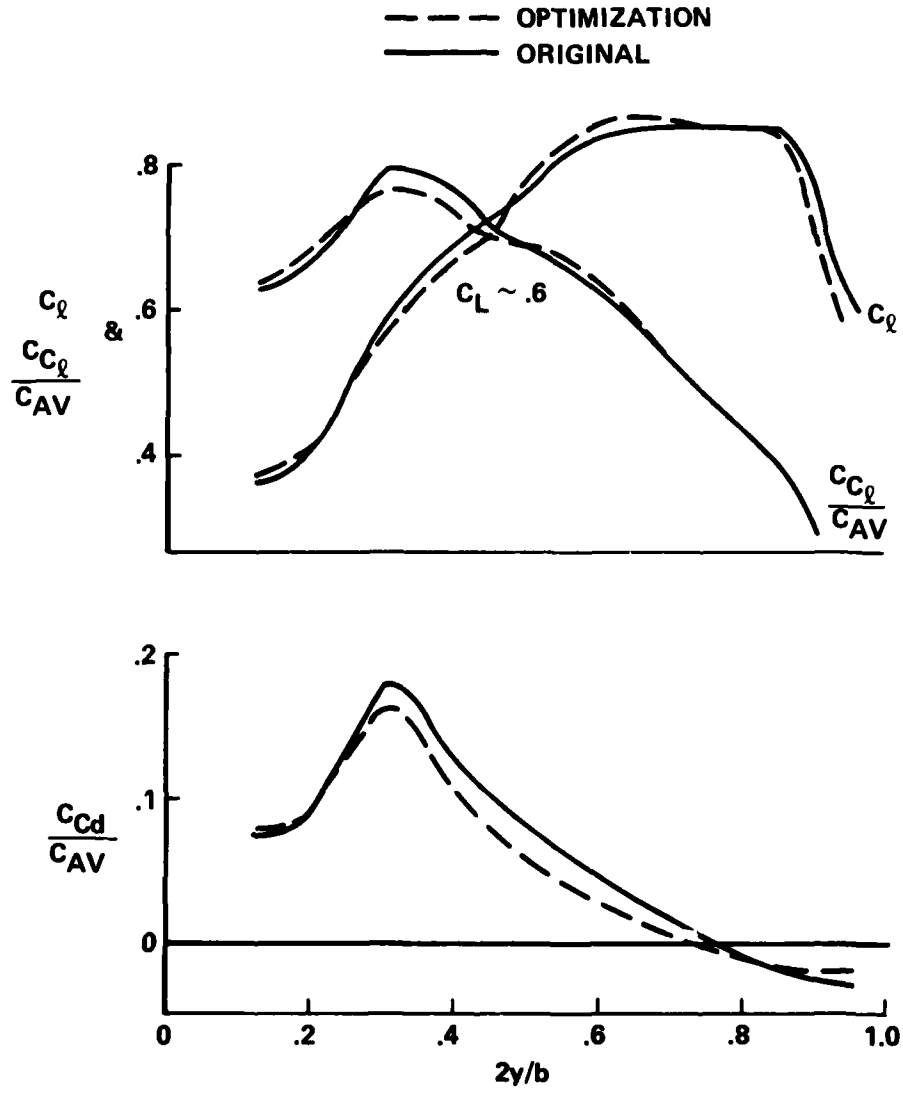

Figure 17. Initial optimization results

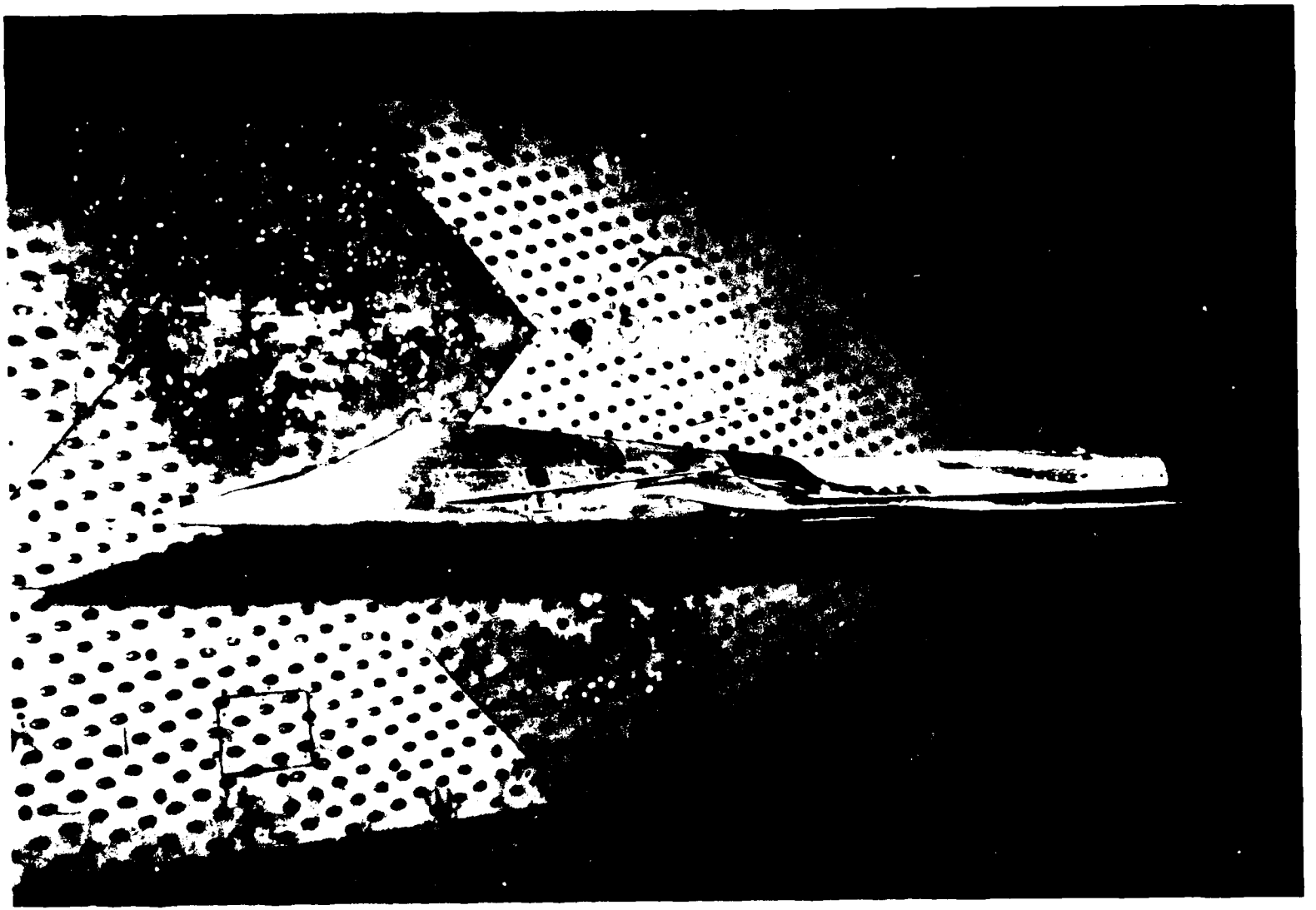

Figure 18. Wind tunnel model in AEDC PWT 16T tunnel

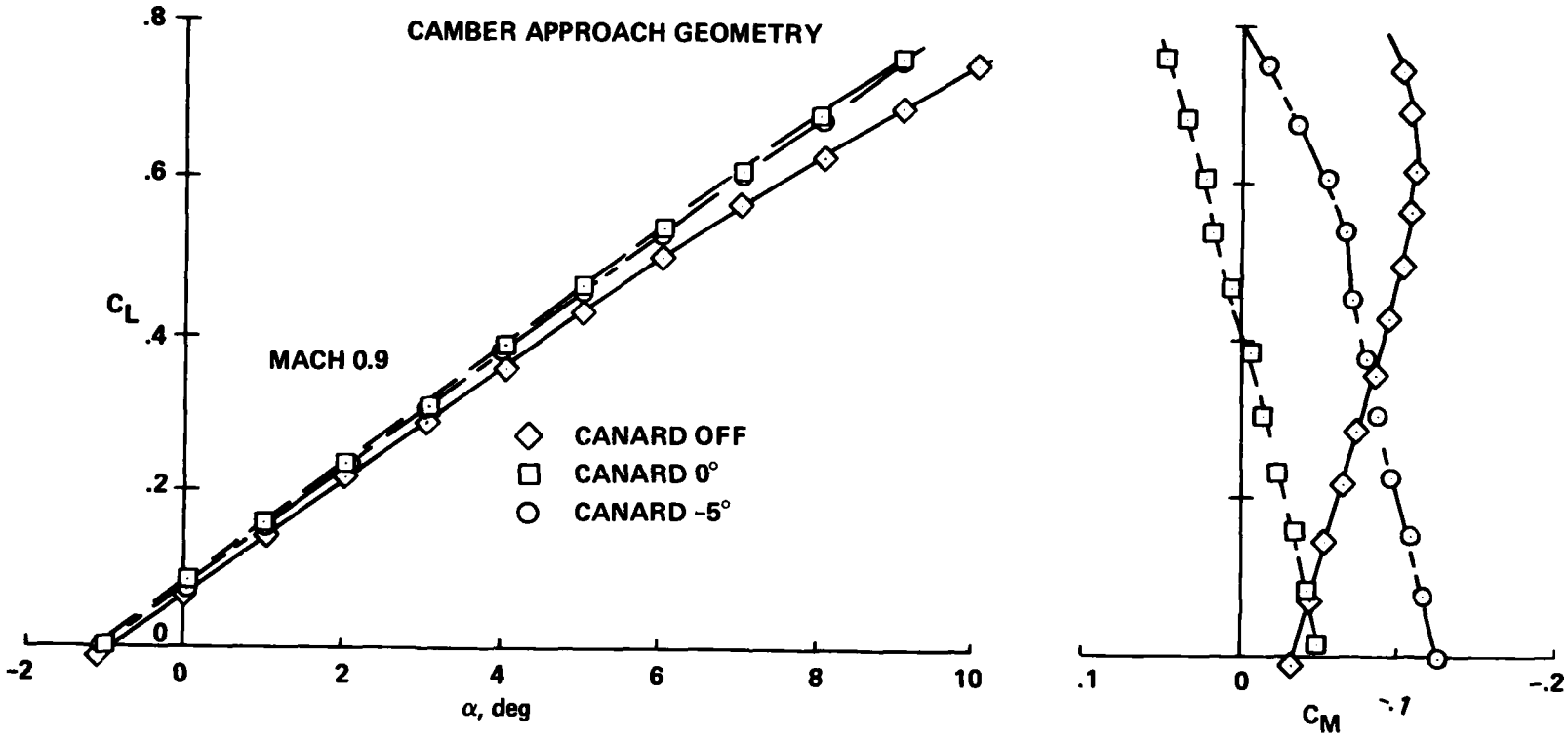

Figure 19. Test results for camber approach geometry, lift and moment summary, Mach 0.9

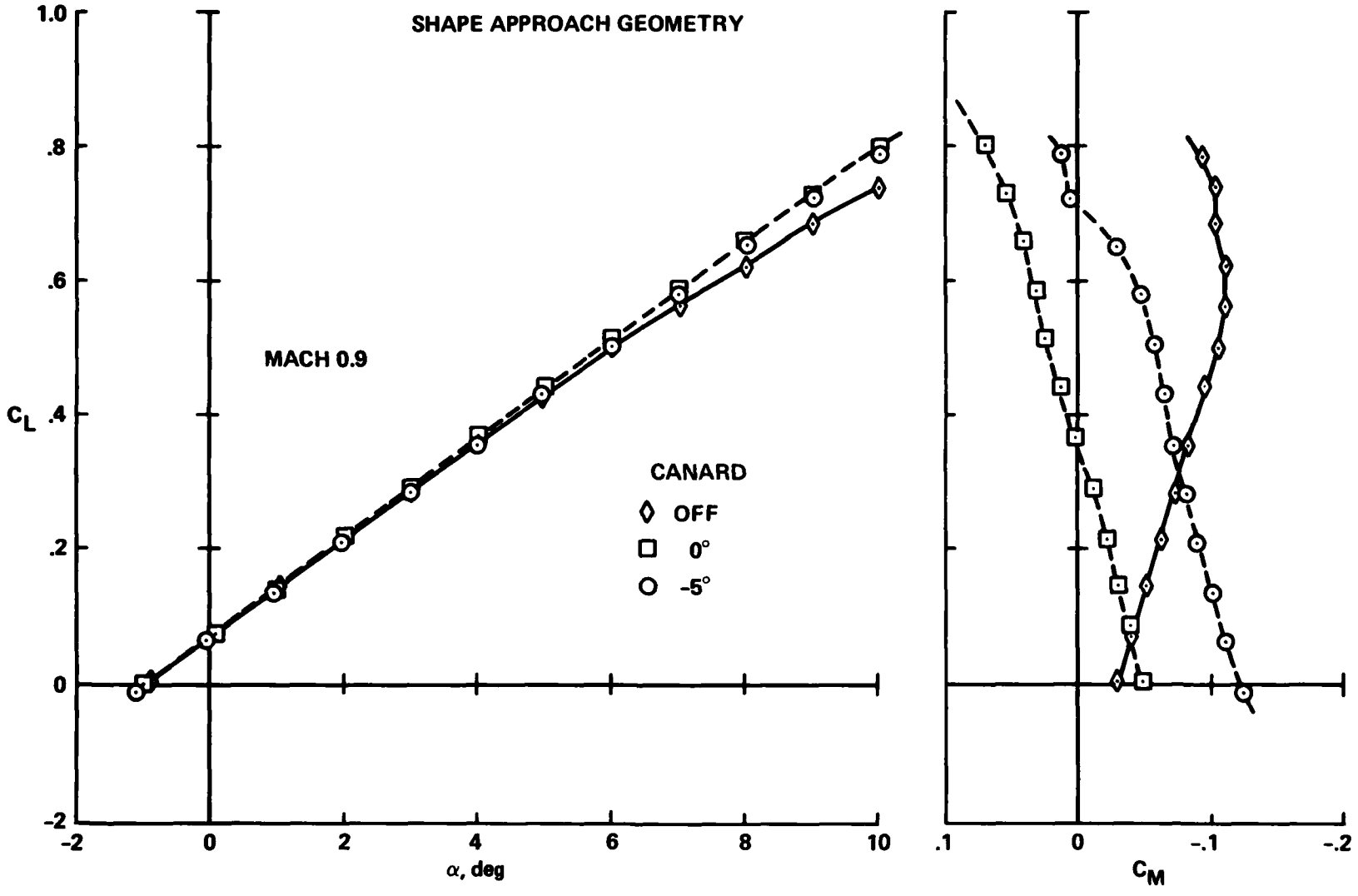

Figure 20. Test results for shape approach geometry, lift and moment summary, Mach 0.9

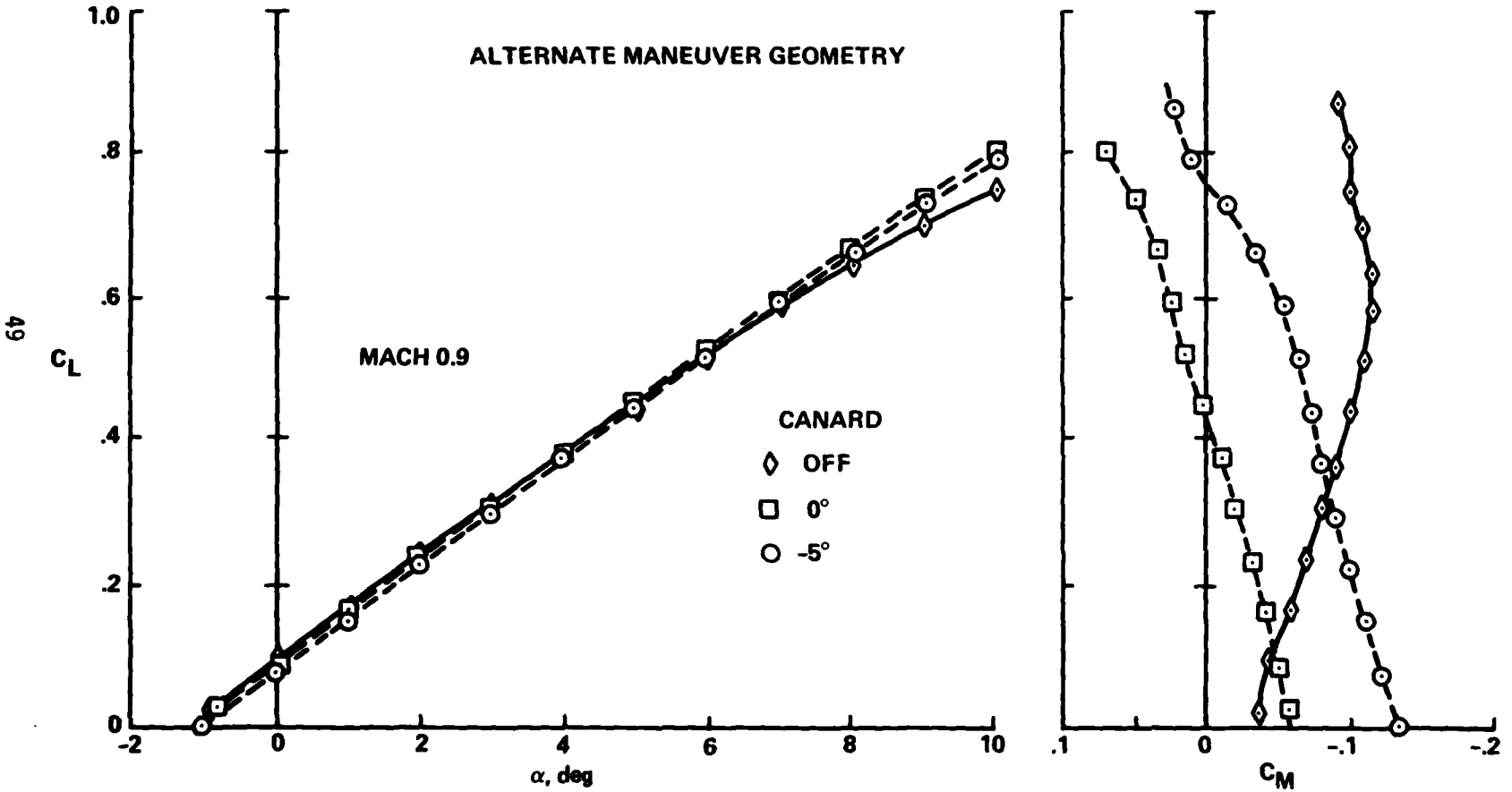

Figure 21. Test results for alternate maneuver geometry, lift and moment summary, Mach 0.9

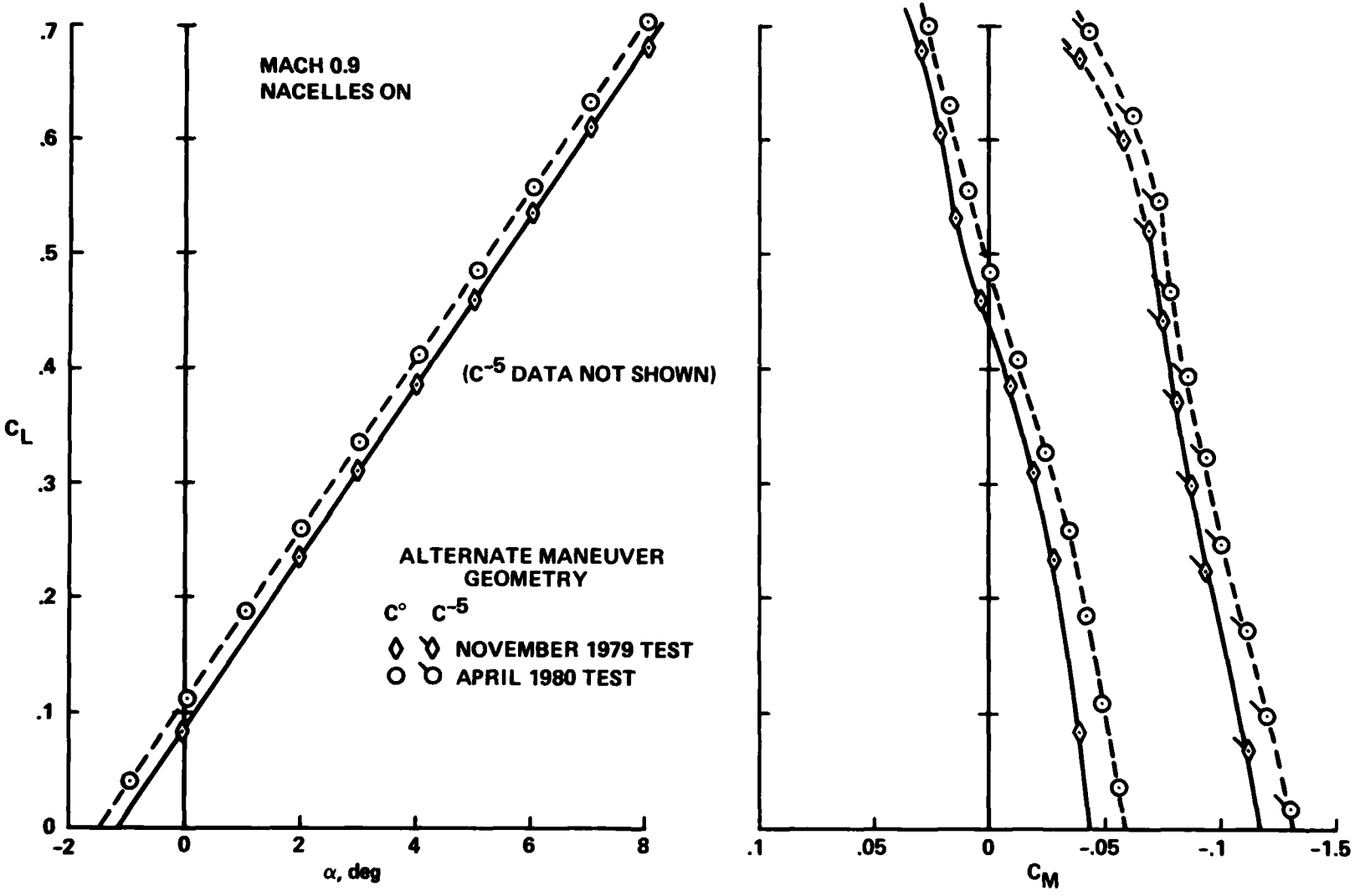

Figure 22a. Comparison of November and April test results, Mach 0.9 - lift and moment

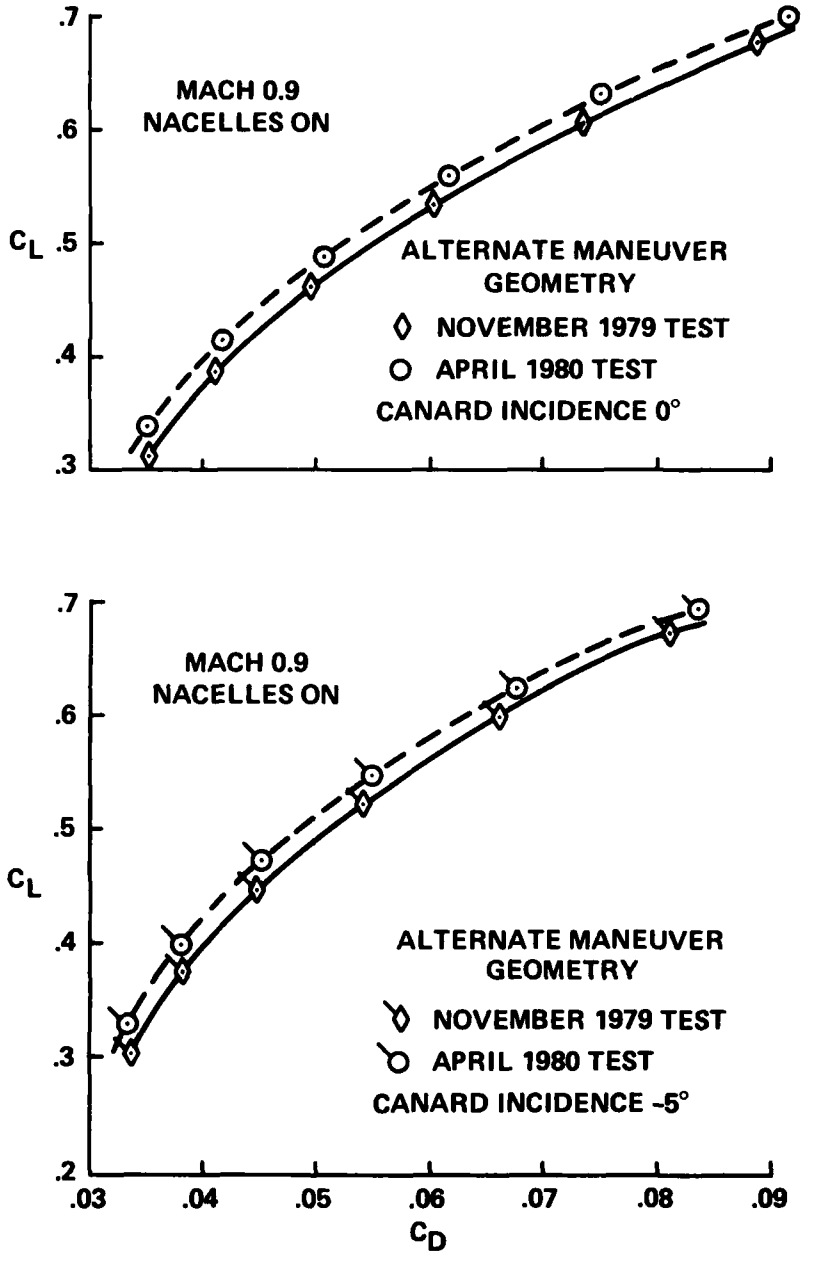

Figure 22b. Comparison of November and April test results, Mach 0.9 - drag

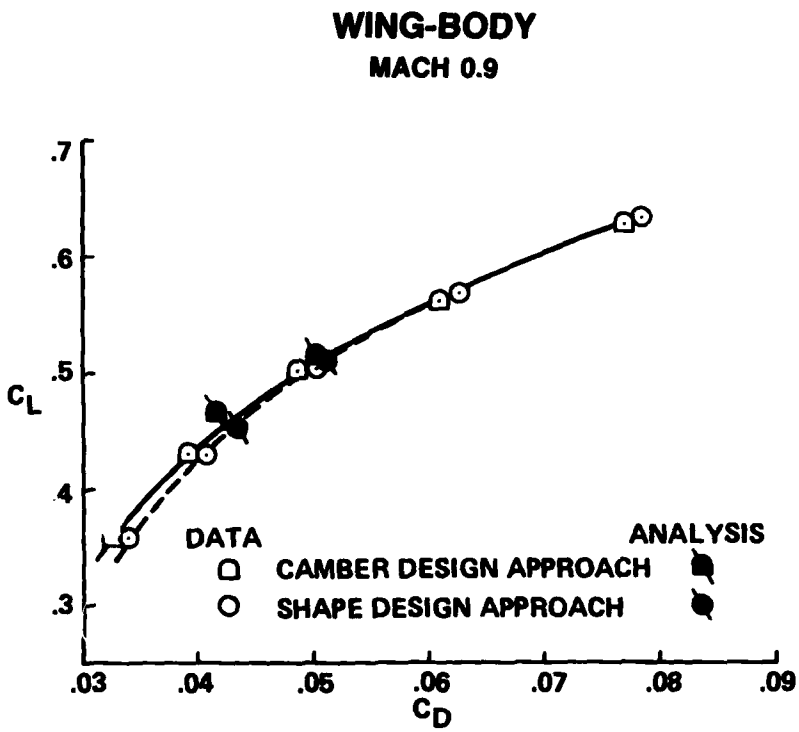

Figure 23. Wing-body drag, data-analysis comparison, Mach 0.9

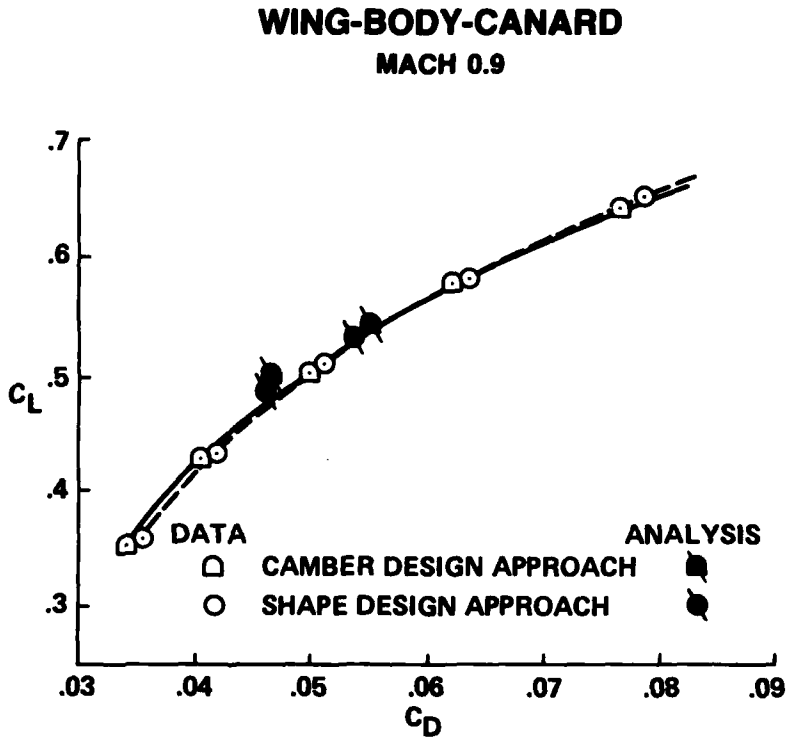

Figure 24. Wing-body-canard drag, data-analysis comparison, Mach 0.9

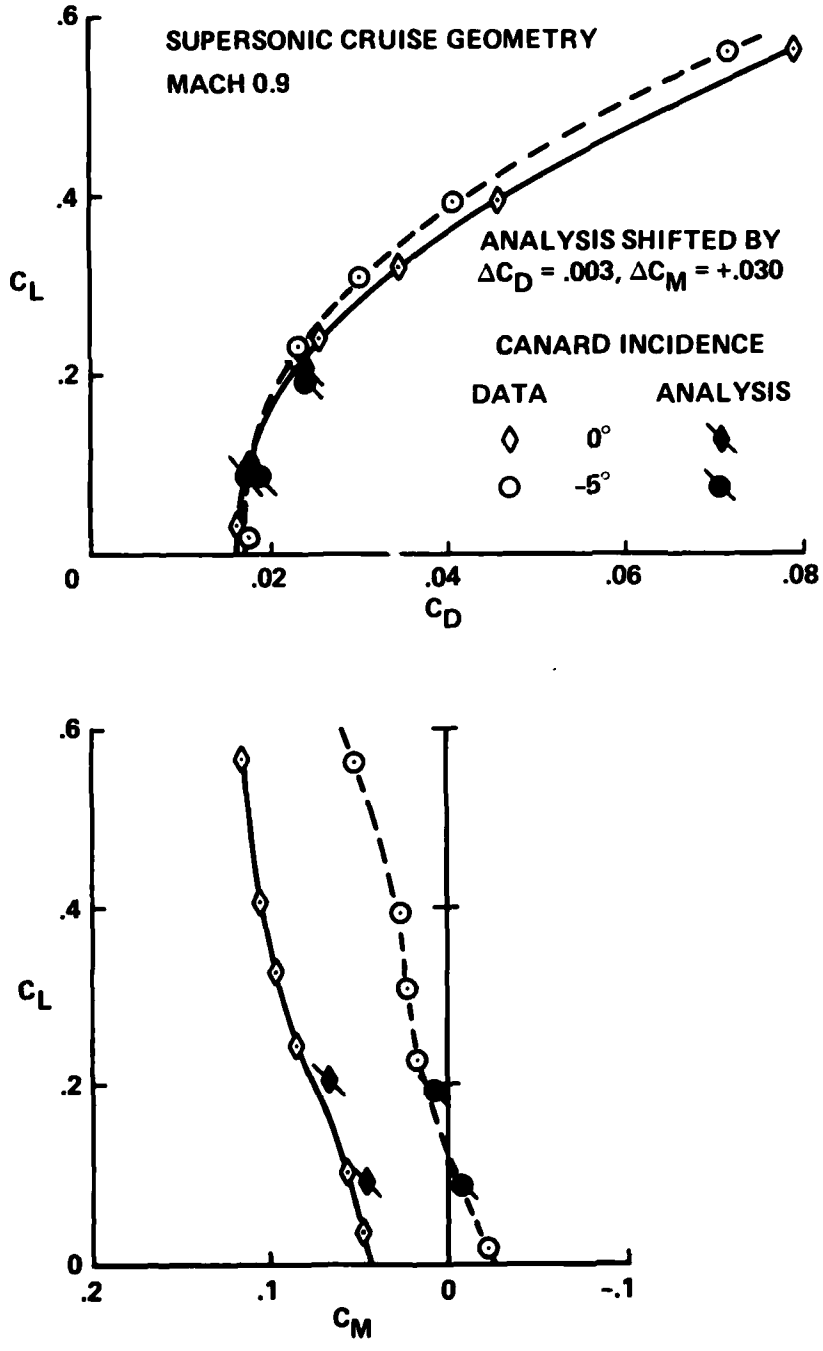

Figure 25. Force and moment changes due to canard incidence, supersonic cruise geometry, Mach 0.9

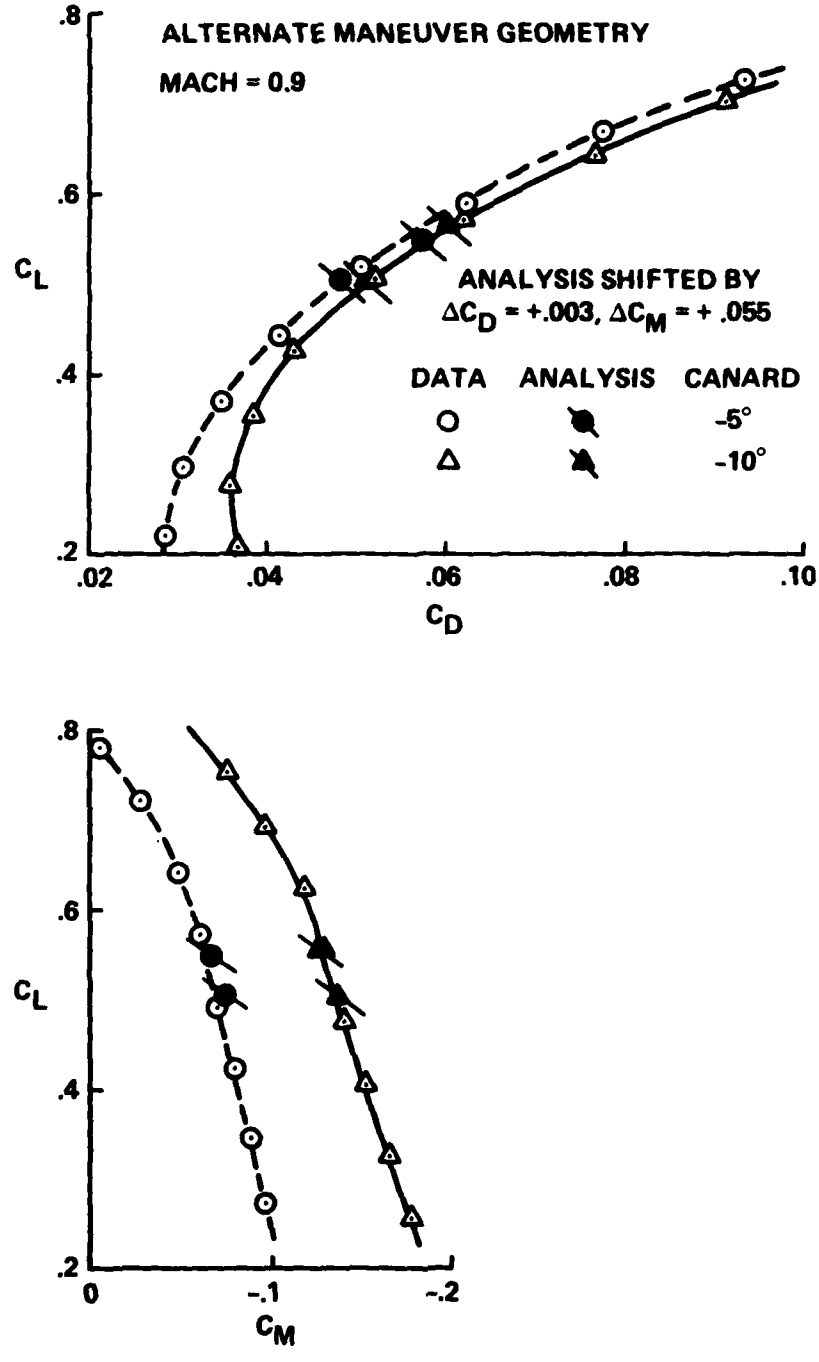

Figure 26. Force and moment changes due to canard incidence, alternate maneuver geometry, Mach 0.9

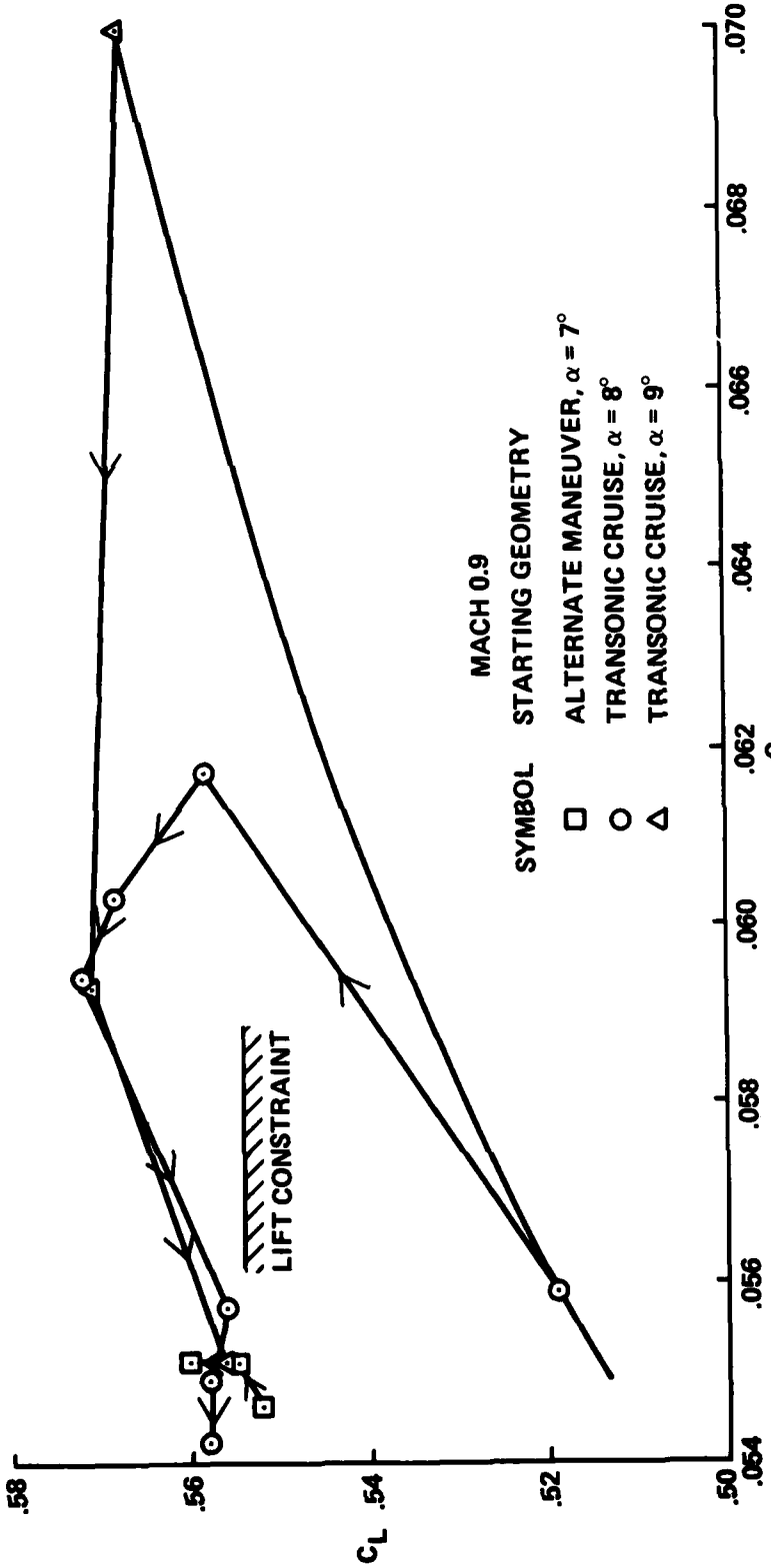

Figure 27. Final design procedure demonstration, L/D maximization, Mach 0.9

*U.S.Government Printing Office: 1981 — 559-005/4024


ILMED
8